TITLE: Fibroblast-expressed LRRC15 suppresses SARS-CoV-2 infection and controls antiviral and antifibrotic transcriptional programs.

Authors

Lipin Loo[1,11], Matthew A. Waller[1,11], Cesar L. Moreno[1], Alexander J. Cole[2], Alberto Ospina Stella[3], Oltin-Tiberiu Pop[4], Ann-Kristin Jochum[4,5], Omar Hasan Ali[4,6,7], Christopher E. Denes[1], Zina Hamoudi[1], Felicity Chung[1], Anupriya Aggarwal[3], Jason K. K. Low[8], Karishma Patel[8], Rezwan Siddiquee[8], Taeyoung Kang[9], Suresh Mathivanan[9], Joel P. Mackay[8], Lukas Flatz[4,10], Daniel Hesselson[2], Stuart Turville[3], G. Gregory Neely[1,12]

Affiliations

[1]Charles Perkins Centre, Dr. John and Anne Chong Lab for Functional Genomics, Centenary Institute, and School of Life and Environmental Sciences, University of Sydney, Camperdown, NSW, Australia.

[2]Centenary Institute and Faculty of Medicine and Health, The University of Sydney, Sydney, NSW, 2006, Australia

[3]The Kirby Institute, University of New South Wales, New South Wales, Australia.

[4]Institute for Immunobiology, Kantonsspital St. Gallen, St. Gallen, Switzerland

[5]Institute for Pathology, Kantonsspital St. Gallen, St. Gallen, Switzerland

[6]Department of Medical Genetics, Life Sciences Institute, University of British Columbia, Vancouver, British Columbia, Canada.

[7]Department of Dermatology, University Hospital Zurich, University of Zurich, Zurich, Switzerland.

[8]School of Life and Environmental Sciences, The University of Sydney, Sydney, New South Wales 2006, Australia.

[9]Department of Biochemistry and Genetics, La Trobe Institute for Molecular Science, La Trobe University, Melbourne, VIC, Australia.

[10]Center for Dermatooncology, Department of Dermatology, Eberhard Karls University of Tübingen, Tübingen, Germany

[11]These authors contributed equally

[12]Lead contact

*Correspondence: greg.neely@sydney.edu.au (G.G.N.)

Abstract

Although ACE2 is the primary receptor for SARS-CoV-2 infection, a systematic assessment of host factors that regulate binding to SARS-CoV-2 spike protein has not been described. Here we use whole genome CRISPR activation to identify host factors controlling cellular interactions with SARS-CoV-2. Our top hit was a *TLR*-related cell surface receptor called *leucine-rich repeat-containing protein 15* (*LRRC15*). *LRRC15* expression was sufficient to promote SARS-CoV-2 Spike binding where they form a cell surface complex. *LRRC15* mRNA is expressed in human collagen-producing lung myofibroblasts and LRRC15 protein is induced in severe COVID-19 infection where it can be found lining the airways. Mechanistically, LRRC15 does not itself support SARS-CoV-2 infection, but fibroblasts expressing LRRC15 can suppress both pseudotyped and authentic SARS-CoV-2 infection in *trans*. Moreover, LRRC15 expression in fibroblasts suppresses collagen production and promotes expression of IFIT, OAS, and MX-family antiviral factors. Overall, LRRC15 is a novel SARS-CoV-2 spike-binding receptor that can help control viral load and regulate antiviral and antifibrotic transcriptional programs in the context of COVID-19 infection.

Keywords

host defense, LRRC15, SARS-CoV-2, COVID-19, Spike, CRISPR activation screen, fibrosis, antiviral response

Introduction

The Coronavirus 2019 (COVID-19) pandemic, caused by SARS-CoV-2, represents the greatest public health challenge of our time. As of October 2022, there have been over 620,000,000 reported cases of COVID-19 globally and more than 6,500,000 deaths (WHO). SARS-CoV-2 shows high sequence similarity (79.6%) with severe acute respiratory syndrome coronavirus (SARS-CoV-1), and because of this similarity, angiotensin-converting enzyme 2 (ACE2), the primary entry receptor for SARS-CoV-1, was quickly identified as the SARS-CoV-2 Spike receptor[1–4]. However, a comprehensive search for other host factors that promote SARS-CoV-2 Spike binding has not yet been reported.

To identify novel host factors that can influence cellular interactions with the SARS-CoV-2 Spike protein, we used a whole genome CRISPR activation approach. Using the Calabrese Human CRISPR Activation Pooled Library[5], we identified a TLR-related cell surface receptor named leucine-rich repeat-containing protein 15 (LRRC15) as a novel SARS-CoV-2 Spike binding protein in three independent whole genome screens, and confirmed this interaction via flow cytometry, immunoprecipitation and confocal microscopy. *LRRC15* is primarily expressed in innate immune barriers including placenta, skin, and lymphatic tissues as well as perturbed-state tissue fibroblasts, and we found LRRC15 protein is absent in control lungs, but highly expressed in COVID-19 patients, where it lines the airways. Mechanistically, LRRC15 is not a SARS-CoV-2 entry receptor, but can antagonise SARS-CoV-2 infection of $ACE2^{+}$ cells when expressed on nearby cells. At the cellular level, LRRC15 is expressed in fibroblasts and these cells increase with COVID-19 infection. Moreover, by RNA seq, we found expression of LRRC15 drives a specific

antiviral response in fibroblasts while suppressing collagen gene expression. In summary, we show LRRC15 physically links SARS-CoV-2 to perturbed-state fibroblasts, where LRRC15 expression can control the balance between fibrosis and antiviral responses, and this activity may help promote COVID-19 resolution while preventing COVID-19 lung fibrosis.

Results

High throughput SARS-CoV-2 Spike binding assay

Based on *a priori* knowledge of SARS-CoV-1, ACE2 was rapidly identified as the primary receptor for SARS-CoV-2 Spike protein[3]. To investigate other host factors that modulate cellular interactions with SARS-CoV-2 Spike, we employed a pooled CRISPR activation (CRISPRa) screening approach. To this end, we developed a novel cellular flow cytometry-based SARS-CoV-2 Spike binding assay using Alexa Fluor 488-labeled Spike protein (Spike488; **Fig. 1a**). While wild-type HEK293T (WT HEK293T) cells that express low levels of ACE2 show minimal binding to Spike488, when we provided *ACE2* cDNA HEK293T-*ACE2* cells exhibited high Spike488 binding activity (**Fig. 1b**). To assess the sensitivity of this assay, we mixed HEK293T-*ACE2* and WT HEK293T cells at various ratios and then measured Spike488 binding by flow cytometry. An increase in Spike488-binding cells could be detected when as little as 1% of the total population was $ACE2^{+}$, indicating that this assay has sufficient sensitivity to enable genome-wide screens (**Fig. 1c**). To perform a pooled CRISPRa screen with this system, we generated a stable HEK293T cell line expressing CRISPRa machinery (*MS2-p65-HSF* + *VP64*; HEK293T-CRISPRa) (**Fig. 1d**). We tested HEK293T-CRISPRa clones for the ability to induce *ACE2* expression using 3 independent single guide RNAs (sgRNAs)[6]. We selected Clone 1 for further use, since it induced

similar levels of *ACE2* expression compared to cDNA overexpression, (**Supplementary Fig. 1a**), and confirmed that CRISPRa induction of ACE2 expression conferred Spike488 binding by flow cytometry (**Fig. 1e**).

CRISPR activation screening for regulators of SARS-CoV-2 Spike binding identifies LRRC15

Having established the utility of our system, we used the Calabrese Human CRISPR Activation Pooled guide Library[5] to drive CRISPRa-dependent expression of the human genome in HEK293T-CRISPRa cells. Cells were infected with lentivirus-packaged CRISPRa sgRNAs and then selected on puromycin to enrich for transduced cells. Transduced cells were incubated with Spike488 and sorted by FACS to isolate CRISPRa-*sgRNA* cells with enhanced Spike binding. Overall, pooled CRISPRa-*sgRNA* cells showed more Spike binding than mock-transduced controls (**Supplementary Fig. 1b-c**). Genomic DNA (gDNA) was collected from unselected or Spike488-selected cells and sgRNA abundance quantified by sequencing (**Fig. 2a**) and then data analyzed using the MAGeCK analysis platform (v0.5.9.2)[7] and plotted using MAGeCKFlute (v1.12.0)[8]. Using an FDR cut off of 0.25, our top hit was the transmembrane protein LRRC15 (LogFC 4.748, P value 2.62×10^{-7}, FDR 0.00495), followed by the SARS-CoV-2 entry receptor ACE2 (LogFC 2.1343, P value 2.65×10^{-5}, FDR 0.25). (**Fig. 2b-d; Supplementary Table 1**). Moreover, we conducted 2 additional screens under slightly different conditions, and in all screens our top hit was LRRC15 (**Supplementary Fig. 2a-f**).

We expressed the *LRRC15* sgRNAs that were hits in our screens in HEK293T-CRISPRa cells and confirmed that they induce expression of *LRRC15* (~approximately 2000-fold induction, **Supplementary Fig. 2g**). Moreover, LRRC15-overexpressing cells dramatically increased SARS-

CoV-2 Spike488 binding, with *LRRC15* sgRNA 1 inducing binding to levels comparable to cells overexpressing *ACE2* sgRNA3 (**Fig. 2e**). LRRC15 overexpression did not itself upregulate *ACE2* transcription, suggesting the increased Spike binding in LRRC15-expressing cells is independent of ACE2 upregulation (**Supplementary Fig. 2h**). Conversely, only one of the three *ACE2* sgRNAs from the Calabrese library efficiently activated *ACE2* expression (**Supplementary Fig. 2i-j**), explaining why *ACE2* itself was not a higher ranked hit in our 3 CRISPRa screens (**Fig. 2d, Supplementary Fig. 2a-f**). To avoid spectral overlap with GFP-expressing cell lines we conjugated Spike with Alexa Fluor 647 (Spike647), which was used for the rest of the study. Using *ACE2* sgRNA3 and *LRRC15* sgRNA1 cells, we measured 11.6 nM affinity for ACE2/Spike647, which is similar to previous estimates (range: 4.7 - 133.3 nM[9–11]) and 68.8 nM for LRRC15/Spike647 (**Fig. 2f**).

LRRC15 is a new transmembrane SARS-CoV-2 Spike receptor

LRRC15 is a 581 amino acid (a.a.) leucine-rich repeat (LRR) protein with 15 extracellular LRRs followed by a single transmembrane domain and a short 22 a.a. intracellular domain (**Fig. 3a and 3b**). LRRC15 belongs to the LRR Tollkin subfamily that includes TLR1-13 and is most closely related to the platelet von Willebrand factor receptor subunit Glycoprotein V (GP5)[12] (**Fig. 3c**, full tree in **Supplementary Fig. 3a**). To confirm a role for LRRC15 in SARS-CoV-2 Spike binding and ensure the interaction was not an artifact of our CRISPRa strategy, we transfected *LRRC15-GFP* cDNA into HEK293T cells and observed Spike647 binding by flow cytometry. There are two reported isoforms of LRRC15 (LRRC15_1 and LRRC15_2), with LRRC15_1 having 6 additional amino acids at the N-terminus. Although cells transfected with *GFP* alone showed no binding to Spike647, cells expressing *LRRC15* isoform 1 or 2 both showed strong Spike binding

(**Fig. 3d**). While LRRC15-dependent Spike binding was higher than cells stably expressing ACE2 (62.1% and 64.5% vs. 48.8%), co-expression of LRRC15 with ACE2 was additive resulting in 86.3% positive (LRRC15_1) or 83.8% positive (LRRC15_2) cells (**Fig. 3e**). Interestingly, all cells (100%) stably expressing ACE2 and TMPRSS2 bound Spike647 regardless of LRRC15 expression (**Fig. 3f**). However, LRRC15 expression in HEK293T-*ACE2*-*TMPRSS2* cells still enhanced the amount of cell surface Spike647 bound by each cell as measured by mean fluorescence intensity (**Fig. 3g**). Moreover, both *LRRC15* isoforms colocalized with Spike647 (**Fig. 3h**). To independently confirm an interaction between LRRC15 and SARS-CoV-2 Spike protein, we added Spike to LRRC15-expressing cells, immunoprecipitated LRRC15, then blotted for both LRRC15 and Spike. While control *GFP*-transfected HEK293T cells did not show any signal at the size predicted for Spike (~200 kDa[13]) (**Supplementary Fig. 3b-c**), when we pulled down either LRRC15_1 or LRRC15_2, in both cases we co-immunoprecipitated Spike protein in the eluate (**Fig. 3i**). Taken together, these data show that LRRC15 expression is sufficient to confer SARS-CoV-2 Spike binding to HEK293T cells, and LRRC15 can further enhance Spike interactions in the presence of ACE2 and TMPRSS2.

LRRC15 is not a SARS-CoV-2 entry receptor but can suppress Spike-mediated entry

We next asked if LRRC15 can act as a receptor for SARS-CoV-2 and mediate viral entry. For this we used a SARS-CoV-2 pseudotyped lentivirus system (SARS-CoV-2 pseudovirus) that displays the SARS-CoV-2 Spike protein and carries a luciferase reporter. LRRC15 did not confer SARS-CoV-2 pseudovirus tropism in HEK293T WT (**Supplementary Fig. 4a**) and HEK293T-*ACE2* cells across a wide range of LRRC15 or pseudovirus doses (**Supplementary Fig. 4b**). We then tested if LRRC15 expression impacted infection of HEK293T-*ACE2* and HEK293T-*ACE2*-

TMPRSS2 cells. Indeed, LRRC15-expression in HEK293T-*ACE2* or HEK293T-*ACE2-TMPRSS2* cells show a relatively strong ability to suppress SARS-CoV-2 pseudovirus infection (**Supplementary Fig. 4c-d**). Next we tested if LRRC15 expression can also suppress viral replication and cytopathic effect in infection with authentic SARS-CoV-2 virus. HEK293T-*ACE2-TMPRSS2* cells were infected with increasing doses of SARS-CoV-2 (Wuhan variant, **Supplementary Fig. 4e**) and cell death was assessed 48 h later. Ectopic expression of LRRC15 did not inhibit infection (two-way ANOVA, $p = 0.378$). Together, these data show that LRRC15 is not sufficient to confer SARS-CoV-2 tropism. Instead LRRC15 can limit SARS-CoV-2 spike-mediated entry in *cis*, but once replication competent virions have entered cells, LRRC15 cannot protect infected cells from death.

LRRC15 is found on lung fibroblasts that are not infected by SARS-CoV-2

At the tissue level, *LRRC15* RNA is most abundant in the placenta, with expression also found in skin, tongue, tonsils, and lung[14]. At the single cell level, we used the COVID-19 Cell Atlas data set to confirm *LRRC15* expression in placenta decidua stromal cells[15], multiple lymphatic vessels[16–19], and fibroblasts from the skin[20], prostate[21] and lung[17,22–26] (**Fig. 4a**). In the lung[26] (**Fig. 4b**), we found *LRRC15* is primarily expressed in fibroblasts as well as a population annotated as "neuronal cells" (**Fig. 4c**), and these populations were not infected with SARS-CoV-2 (**Fig. 4d**). These data were corroborated by two other COVID-19 patient single cell/nucleus RNAseq data sets that show similar *LRRC15* fibroblast expression profiles (**Supplementary Fig. 5a-f**), and again $LRRC15^{+}$ cells were not infected with SARS-CoV-2[24] (**Supplementary Fig. 5c**). Of note, the viral RNA detected was low in these patients. Together, these data support our *in vitro* observations that LRRC15 does not mediate SARS-CoV-2 infection but may instead act as an

innate immune barrier. In contrast, ACE2 was detected primarily in uninfected type I (AT1) and (AT2) alveolar epithelium (**Fig. 4d)**, and SARS-CoV-2-infected alveolar epithelium ("Other epithelial cells") that lost AT1/2 markers and upregulated ribosomal transcripts consistent with viral infection and cell death. We next assessed LRRC15 protein expression in human lung parenchyma. We observed that COVID lungs have epithelial metaplasia, more immune infiltrate and intra alveolar fibroblast proliferation (**Fig. 4e-f, Supplementary Fig. 6a**). This matches with single cell RNA seq that shows lung fibroblasts increases significantly during COVID-19 (7.9% in control and 22.9% in COVID-19 patients; **Fig. 4g**). Moreover, we found that LRRC15 is present on the alveolar surface of lung tissue samples from donors with COVID-19, but not present in control lungs from individuals without COVID-19, and LRRC15 expression was mutually exclusive with collagen (**Fig. 4h-i, Supplementary Fig. 6b)**.

While HEK293T cells do not express *LRRC15*, the human fibroblast line IMR90 does (**Fig. 5a**). In the rat glia cell line C6 *LRRC15* is mildly regulated in response to proinflammatory cytokines like IL1β, IL6, and TNFα[27], and more recently TGFβ signalling has been linked to LRRC15 expression in cancer-associated fibroblasts[28,29]. In human fibroblasts, we found IL1β, TNFα or IFNɣ do not induce detectable levels of LRRC15 (not shown), however TGFβ upregulates both *LRRC15* (**Fig. 5b**) and *COL1A1* transcripts (**Fig. 5c**) and LRRC15^{+} fibroblasts bind SARS-CoV-2 Spike protein (**Supplementary Fig. 7a**). Moreover, ectopic expression of LRRC15 is also sufficient to enhance SARS-CoV-2 Spike binding on fibroblasts (**Fig. 5d**), however LRRC15 expression was again not sufficient to confer SARS-CoV-2 pseudovirus tropism (**Fig. 5e)**. Since human lung fibroblasts express LRRC15 and are not infected with SARS-CoV-2, we reasoned that LRRC15 may act to bind and sequester SARS-CoV-2 virions away from ACE2^{+} target lung

epithelium. In human COVID-19 patients, fibroblasts and epithelial cells are present at a ratio of ~2:1 (**Fig. 5f**). Thus to test if LRRC15 can sequester virus and suppress SARS-CoV-2 infection, we co-cultured fibroblasts expressing *LRRC15-GFP* with SARS-CoV-2 permissive HEK293T-*ACE2-TMPRSS2* at a ratio of 2:1. Indeed we found LRRC15^{+} fibroblasts can antagonise infection of both SARS-CoV-2 pseudovirus (**Fig. 5g**) and authentic SARS-CoV-2 virus (Wuhan, **Fig. 5h**). Thus, together we show LRRC15 is expressed specifically by lung fibroblasts, is found coating the airways in COVID-19 patients, and mechanistically, LRRC15 can act to sequester SASR-CoV-2 virus and help suppress infection, which may potentially help protect ACE2^{+} alveolar epithelium in patients with COVID-19.

LRRC15 is a potent regulator of antiviral and fibrotic programs

While we believe the most direct mechanism by which LRRC15 may participate in COVID-19 infection is through binding to and sequestering SARS-CoV-2 virions, little is known about the broader role for LRRC15 in physiology or how LRRC15 expression impacts fibroblast transcriptional programs. A recent study on the organization of tissue fibroblasts identified *LRRC15* as a lineage marker for perturbed state activated myofibroblasts[23]. These specialized fibroblasts arise during disease, express collagen and other ECM-modifying genes, and participate in tissue repair and fibrosis[23]. We also observed lung *LRRC15*$^{+}$ myofibroblasts in multiple COVID-19 patient data sets, and these cells also express collagen **(Fig. 6a**). To directly investigate the relationship between LRRC15 and collagen, we generated an LRRC15 overexpressing stable human fibroblast line, then evaluated LRRC15-induced transcriptional changes by RNA seq. Surprisingly, we found driving expression of LRRC15 in fibroblasts induced upregulation of

cellular antiviral programs and downregulated expression of collagen transcripts (**Fig. 6b, Supplementary Table 5**). These results are clearly visible in the volcano plot (red transcripts were upregulated, blue transcripts down regulated), however they were also captured in pathway analysis (**Fig. 6c, Supplementary Table 6**), where we found interferon and influenza signalling were the most upregulated pathways, whereas wound healing and pulmonary fibrosis were the most downregulated pathways. Of note, pancreatic adenocarcinoma signalling was also highly upregulated, and this is in line with a recent study highlighting the role of LRRC15^{+} fibroblasts in driving disease severity in pancreatic cancer[29] . The primary antiviral pathways upregulated by LRRC15 expression were IFITs (Interferon Induced proteins with Tetratricopeptide repeats), MXs (Myxovirus resistance genes), and OASs (2-prime, 5-prime oligoadenylate synthetases) and we confirmed these data by RT-qPCR (**Fig. 6d**). Moreover, LRRC15 expression had an unexpected and potent ability to downregulate collagen transcripts, and we confirmed this both by RT-qPCR (**Fig. 6e)** and western blotting (**Fig. 6f, Supplementary Fig. 6b).**

Overall, we describe the TLR-related receptor LRRC15 as a new spike receptor that can bind and sequester SARS-CoV-2 and limit infection. LRRC15 is induced extensively during COVID-19, where it lines the airways and may form an innate antiviral barrier. Surprisingly, while LRRC15 is induced on fibroblasts during disease, ectopic expression of LRRC15 switches fibroblast transcriptional programs from a fibrotic program to an antiviral one, and this may help the lung orchestrate innate immunity programs vs. immune resolution and lung repair.

Discussion

Using an unbiased functional genomics approach, we have identified the leucine rich repeat receptor LRRC15 as a new SARS-CoV-2 inhibitory receptor that can regulate innate immunity and lung repair. LRRC15 promotes SARS-CoV-2 spike binding comparable to ACE2, however LRRC15 is not sufficient to confer viral tropism. LRRC15 is normally highly expressed in tissues that form important immune barriers like the placenta, skin, and various lymphatics, and is related to TLR innate immune receptors[14]. In previous work, LRRC15 has been shown to suppress adenovirus infection[30], and here we show LRRC15 can also bind to and suppress SARS-CoV-2 Spike pseudovirus and live SARS-CoV-2 infection. Moreover, in human SARS-CoV-2-infected airways, we see that LRRC15 forms a pronounced barrier-like structure, and given the expression pattern and function of LRRC15, we hypothesize that this molecule is a pattern recognition receptor and innate immune barrier that may play an important role in host defense. Moreover, LRRC15 is found on collagen-producing myofibroblasts and we show ectopic expression of LRRC15 suppresses collagen production and drives antiviral programs, and in this way directly links SARS-CoV-2 with innate antiviral immunity and lung fibrosis.

Although our data shows that LRRC15 promotes cellular binding to SARS-CoV-2 Spike protein, we also show that LRRC15 does not act as an entry receptor, but instead can inhibit SARS-CoV-2 in *trans*. This observation is consistent with a previous report that LRRC15 can also impede adenovirus infection[30]. We hypothesize that LRRC15 may play a role in limiting SARS-CoV-2 transmission by sequestering free virus in the airways of COVID-19 patients, and the LRRC15 we observed lining the airways may also suppress collagen deposition protecting the airways from fibrosis during some stages of lung infection. It is likely that the role for LRRC15 in lung immunity is more broad than just interactions with SARS-CoV-2, and LRRC15 may represent a new

284 fibroblast-expressed pattern recognition receptor that can bind to and sequester a variety of
285 microbial antigens, however this remains to be established.
286
287 LRRC15 is a member of the LRR superfamily and LRR-Tollkin subfamily of LRR-containing
288 proteins, many of which play critical roles in host defense[12]. Of the TLR family, LRRC15 is most
289 related to TLR5, which also recognises a major extracellular virulence factor, the bacterial
290 extracellular protein flagellin[31]. Remarkably, while our manuscript was in preparation and then
291 review, two other groups independently released preprints describing similar ORF/CRISPR
292 activation screening strategies to identify new host factors that can regulate Spike binding; both
293 screens also pulled out LRRC15 as a top factor driving Spike/host cell interactions[32,33]. These
294 studies corroborate our findings, despite their use of different Spike formulations, overexpression
295 strategies, and cell lines. Moreover, since our initial submission[34], Song et al. have replicated our
296 finding that LRRC15 can act in *trans* to suppress SARS-CoV-2 infections and this has now been
297 published[33]. Together, our studies highlight a fundamental new role for LRRC15 in SARS-CoV-2
298 biology and likely beyond.
299
300 Several CRISPR Loss of Function (LOF) and Gain of Function (GOF) screens have been reported
301 in attempts to identify novel SARS-CoV-2 interactors and regulators. Though these CRISPR
302 screens have been successful in identifying novel SARS-CoV-2 receptors and co-receptors[35–39],
303 ACE2-regulators[40,41], complexes such as the vacuolar ATPase proton pump, Retromer,
304 Commander and SWI/SNF chromatin remodeling machinery[40,41] and have implicated many new
305 pathways in SARS-CoV-2 infection[36,38,41], they have all failed to identify LRRC15. This difference
306 is likely due to screening with SARS-CoV-2 authentic virus and pseudovirus screens being unable

to divorce Spike binding from downstream effects of infection. Our fluorophore-conjugated Spike protein/pooled CRISPR screening model thus represents a new and complementary paradigm for investigating host/virus interactions or virtually any other cell surface interaction.

Our data suggests the primary mechanism of action for LRRC15 in the context of SARS-CoV-2 infection is likely through a direct interaction with the Spike protein that sequesters SARS-CoV-2 virions and in this way helps to limit infection. Beyond this, we show that LRRC15 also has a potent and specific impact on fibroblast gene expression, suppressing collagen while enhancing antiviral programs. We found LRRC15 expression caused an upregulation of 3 antiviral pathways, IFIT, MX, and OAS, and these antiviral pathways are also upregulated in primates infected with SARS-CoV-2[42] and COVID-19 patients[43]. IFIT proteins are induced by IFN, viral infection, or PAMP recognition, where they can then directly bind to viral RNA, block viral translation, and activate cellular antiviral responses[44]. A recent preprint found the SARS-CoV-2 nonstructural protein NSP16 helps SARS-CoV-2 evade the host antiviral immune response by avoiding the antiviral activities of IFIT1 and 3[45]. MX proteins are interferon-induced dynamin-like GTPases with antiviral activity against multiple RNA and DNA viruses. For example MX1 can block influenza A by altering sorting of viral vesicles in the ER / Golgi intermediate compartment[46]. In COVID-19, MX1 is upregulated with increasing viral load[47], and functionally, the SARS-CoV-2 protein ORF6 can suppress MX1 induction[48]. OAS proteins are dsRNA sensors that can activate RNAse L which then degrades viral RNA and inhibits protein synthesis[49]. Importantly, OAS1 is a potent host antiviral factor that can block SARS-CoV-2 infection *in vitro*, and OAS1 expression also associates with protection from severe COVID-19 outcome *in vivo*[50].

While our data highlights a new role for LRRC15 in promoting SARS-CoV-2 Spike binding, limiting infection, and regulating collagen expression, it is currently unclear how LRRC15 contributes to human COVID-19 disease. Notably, while this manuscript was under revision, a preprint authored by Gisby et al. investigated serum from control and COVID-19 infected end stage kidney disease patients, and found that out of the entire serum proteome, depletion of circulating LRRC15 is the strongest predictor of COVID-19 clinical outcome[51]. Integrating these data, it is possible that fibroblast-expressed LRRC15, or potentially cell free LRRC15 deposits in the airways, could trap viral particles for subsequent clearance by the innate immune system, while at the same time enhancing cellular antiviral tone and suppressing fibrosis. LRRC15 may even help fibroblasts pass immobilized virus to innate lung antigen presenting cells, as a recent spatial transcriptomics study showed that lung fibroblasts interact with both SARS-CoV-2 Spike^{+} macrophages and dendritic cells[52]. If lung LRRC15/SARS-CoV-2 complexes are depleted, and new LRRC15 is not produced, this may lead to a detectable decrease in serum LRRC15 that is indicative of poor COVID-19 outcome. While it is clear that LRRC15 is an important new component of our innate immune system, the precise mechanisms of action of LRRC15 during COVID-19 infection remain to be established.

Overall, our unbiased functional genomic investigation of SARS-CoV-2 Spike/host interactions identified the novel TLR-related receptor LRRC15 as a powerful host factor driving SARS-CoV-2 Spike interactions and controlling both antiviral and anti-fibrotic responses. Further investigation into how LRRC15 contributes to innate immunity can help us better understand and treat this and future pandemics.

353 **Lead contact**

354 Further information and requests for resources and reagents should be directed to and will be
355 fulfilled by the lead contact, Graham G. Neely (greg.neely@sydney.edu.au).

356

357 **Materials availability**

358 This study did not generate any new unique reagents.

359

360 **Data and code availability**

361 CRISPR screen raw read counts have been deposited at GSE186475 and are publicly available as
362 of the date of publication. CRISPR screen analysis is shown in **Fig. 2** and **Supplementary Fig. 2.**
363 CRISPR screen output is reported in **Supplementary Table 1**. RNA sequencing bam files have
364 been deposited on NCBI SRA at PRJNA895078 and are publicly available as of the date of
365 publication. Analysis of RNA sequencing data is shown in **Fig. 6**. Results of differential gene
366 expression analysis are reported in **Supplementary Table 5**. Canonical Pathways output from
367 Ingenuity Pathway Analysis is reported in **Supplementary Table 6**. This paper also analyzes
368 existing publicly available single cell RNA-sequencing data (GSE158127, SCP1052, SCP1219).
369 All data reported in this paper will be shared by the lead contact upon request. This paper does not
370 report original code. Any additional information required to reanalyze the data reported in this
371 paper is available from the lead contact upon request.

372

373 **Experimental model and subject details**

374

375 **Cell culture**

HEK293T cells (female; ATCC, CRL-3216, RRID: CVCL_0063) were cultured in Dulbecco's Modified Eagle Medium (ThermoFisher Scientific, Cat #11995065) with 10% HyClone Fetal Bovine Serum (Cytiva, SH30084.03) and 1% Penicillin-Streptomycin (Gibco, 15140122) at 37°C, 5% CO_2 and atmospheric oxygen. IMR90 *E6E7* (female) human fibroblast cells were a gift from Anthony Cesare (Children's Medical Research Institute, Sydney, Australia). IMR90 were cultured in DMEM (ThermoFisher Scientific, 11995065) supplemented with 10% HyClone FBS (Cytiva, SH30084.03) and 1x non-essential amino acids (Gibco, 11140050) at 37°C, 3% O_2 and 10% CO_2. Expi293F™ cells (female; ThermoFisher Scientific, A14527, RRID:CVCL_D615) were cultured in Expi293™ Expression Medium (ThermoFisher Scientific, A1435101) with 5% CO_2 and atmospheric O_2 at 37 °C for 24 h and then lowered to 32 °C for 72 h. Cell lines have been authenticated.

Method Details

Generation of CRISPR activation cell line

HEK293T cells were co-transfected with pPB-R1R2_EF1aVP64dCas9VP64_T2A_MS2p65HSF1-IRESbsdpA (Addgene #113341) and the Super PiggyBac Transposase Expression Vector (System Biosciences, PB210PA-1) using Lipofectamine 3000 Transfection Reagent (ThermoFisher Scientific). These cells (HEK293T-CRISPRa) were then selected on blasticidin (Merck) at 5 μg/mL for 10 days prior to clonal isolation and expansion. These cells express synergistic activation machinery (SAM), which includes VP64-dCas9-VP64 fusion protein and helper proteins MS2, p65 and HSF. When

transduced with pXPR_502 (Addgene #96923) single guide RNA (sgRNA) plasmid, the cells also express PCP-p65-HSF complex which is recruited to PP7 aptamers in the sgRNA scaffold [5].

sgRNA vector cloning

Single guide RNA (sgRNA) sequences for non-targeting control and ACE2 were taken from the Weissman Human Genome-wide CRISPRa-v2 library (Addgene #83978). LRRC15 sgRNA sequences and additional ACE2 sgRNA sequences were taken from the Human CRISPR activation pooled library set A (Addgene #92379). Sense and antisense strands for each sequence were ordered as DNA oligonucleotides (IDT) with 5' overhangs of 5'-CACC-3' on the sense strand oligonucleotide and 5'-AAAC-3' on the antisense strand oligonucleotide. Oligonucleotides were annealed at 4°C for 16 h and pXPR-502 (Addgene #96923) was digested with Esp3I (ThermoFisher Scientific, ER0451) or BsmBI-v2 (New England Biolabs). sgRNA DNA oligonucleotide duplexes were ligated into the digested pXPR-502 backbone using T4 ligase (New England Biolabs) and incubated at 4°C overnight. NEB 10-beta competent *E. coli* (New England Biolabs) were transformed with 100 ng of each sgRNA construct by heat-shock, plated onto LB-agar plates (Life Technologies) containing ampicillin (Sigma-Aldrich) and grown at 37°C. Individual colonies were picked, expanded in Luria broth (Life Technologies) supplemented with ampicillin and amplified constructs were harvested using either ISOLATE II Plasmid Mini Kit (Bioline) or PureYield Plasmid Maxiprep System (Promega Corporation).

Whole genome sgRNA library amplification

MegaX DH10B $T1^R$ Electrocomp™ Cells (ThermoFisher Scientific) were electroporated with 400 ng Human CRISPR activation pooled library set A (Addgene #92379) and left to recover in

Recovery Medium for 1 hour at 37°C. Cells were then spread on 600 cm^2 LB-agar plates supplemented with carbenicillin (Merck) and incubated at 37°C for 16 hours. All colonies were scraped, collected and processed using the PureYield Plasmid Maxiprep System (Promega Corporation). The concentration of the plasmid library was determined via Nanodrop (ThermoFisher Scientific).

Lentivirus production and viral transduction

Lipofectamine 3000 Transfection Reagent (ThermoFisher Scientific) in Opti-MEM Medium (Gibco) was used to co-transfect HEK293T cells with psPAX2 (Addgene #12260), pCAG-VSVg (Addgene #35616) and either individual sgRNA constructs ligated into pXPR-502 (Addgene #96923) or pooled CRISPRa library (Human CRISPR activation pooled library set A, Addgene #92379) according to the manufacturer's instructions. Cells were incubated with transfection reagents for 16 h before the media was replaced. Viral media was collected 24 h later. For individual sgRNA constructs, neat viral media was added to HEK293T-CRISPRa cells with Polybrene Infection / Transfection Reagent (Sigma-Aldrich) at a concentration of 8 µg/mL. Viral media was replaced with fresh medium the following day and puromycin dihydrochloride (Gibco) added 24 h later at a concentration of 1.6 µg/mL for 72 h selection. For sgRNA library virus, viral media was passed through a 0.45 µm filter (Merck Millipore) and concentrated using 100K MWCO Pierce Protein Concentrators (Life Technologies Australia). Concentrated virus was then stored at -80°C.

SARS-CoV-2 Spike protein production

443 The expression construct for recombinant soluble trimeric SARS-CoV-2 spike protein (residues
444 1-1208, complete ectodomain) was generously provided by Dr Florian Krammer (Icahn School of
445 Medicine, Mt Sinai). This protein was used for the initial setup of the screen (shown in Fig. 1) and
446 in one CRISPRa screen (Screen 2). This construct includes the SARS-CoV-2 Spike native signal
447 peptide (residues 1-14) to target the recombinant protein for secretion, stabilising proline
448 substitutions at residues 986 and 987, substitution of the furin cleavage site (residues 682-685)
449 with an inert GSAS sequence, and a C-terminal His6-tag to enable affinity purification.
450
451 Soluble trimeric SARS-CoV-2 spike was expressed in EXPI293F™ cells via transient transfection
452 using 25 kDa linear polyethyleneimine (PEI) (Polysciences Inc.). EXPI293F™ cultures were
453 grown at 37°C, with shaking at 130 rpm, to a cell density of $3x10^6$ cells/mL before transfection
454 with pre-formed SARS-CoV-2 spike plasmid DNA:PEI complexes (2 µg/mL DNA and 8 µg/mL
455 PEI). The transfected cells were incubated at 37°C for 24 h and then at 32°C for a further 72 h
456 before harvesting. Culture medium, containing secreted SARS-CoV-2 spike, was harvested by
457 centrifugation at 4000 xg for 20 min. Supernatants from the centrifugation step were supplemented
458 with 20 mM HEPES (pH 8.0) and subjected to immobilised metal affinity chromatography
459 (IMAC) by incubation with Ni-NTA agarose pre-equilibrated with a buffer consisting of 20 mM
460 NaH_2PO_4 (pH 8.0), 500 mM NaCl, and 20 mM imidazole. His6-tagged SARS-CoV-2 spike protein
461 was eluted from the Ni-NTA agarose using a buffer comprising 20 mM NaH_2PO_4 (pH 7.4), 300
462 mM NaCl, and 500 mM imidazole. Eluates from affinity chromatography were concentrated and
463 further purified by gel filtration chromatography using a Superdex 200 10/30 GL column (Cytiva)
464 and buffer consisting of 20 mM HEPES (pH 7.5) and 150 mM NaCl. The quality of protein
465 purification was assessed by SDS-PAGE and multiple angle laser light scattering (MALLS).

The expression construct for a more stable variant of soluble trimeric SARS-CoV-2 spike ectodomain protein called "HexaPro" was a gift from Jason McLellan (Addgene, #154754). This "Hexapro" protein was used in 2 CRISPRa screens (Screen 1 and 3) and in all validation experiments. This construct, in addition to above, includes 6 total stabilising proline substitutions at residues 817, 892, 899, 942, 986 and 987. The protein was expressed, and the culture medium was harvested as above. The supernatant containing the protein was supplemented with 20 mM HEPES pH 8.0 and subjected to IMAC with Ni-NTA as above. The eluate was dialysed to a buffer containing 2 mM Tris (pH 8.0) and 200 mM NaCl and concentrated to reduce the total volume by a factor of 3. The sample was passed through a 0.22 µm filter and purified by gel filtration chromatography using HiLoad 16/600 Superdex 200 (Cytiva) in a buffer composed of 2 mM Tris (pH 8.0) and 200 mM NaCl. The quality of the protein was assessed by SDS-PAGE and MALLS.

Conjugation of SARS-CoV-2 Spike glycoprotein with fluorophores

Spike protein was conjugated to Alexa Fluor™ 488 or Alexa Fluor™ 647 using protein labelling kits (Invitrogen) according to manufacturer's instructions. Briefly, 50 µL of 1 M sodium bicarbonate was added to 500 µl of 2 mg/mL Spike protein. The solution was then added to room temperature Alexa Fluor™ 488 or 647 reactive dye and stirred for 1 h at room temperature. Conjugated Spike proteins were loaded onto Bio-Rad BioGel P-30 Fine size exclusion purification resin column and eluted via gravity (Alexa Fluor™ 488) or centrifugation (Alexa Fluor™ 647). NanoDrop (ThermoFisher Scientific) was used to determine protein concentration.

Generation of ACE2 and dual ACE2/TMPRSS2 cDNA overexpression cell lines

HEK293T cells stably expressing human ACE2 (HEK293T-*ACE2*) were generated by transducing HEK293T cells with a lentivirus expressing *ACE2*[53]. Briefly, ACE2 ORF was cloned into a 3rd generation lentiviral expression vector, pRRLsinPPT.CMV.GFP.WPRE[54] using Age1/BsrG1 cut sites, thus replacing *GFP ORF* with *ACE2* to create a novel expression plasmid, herein referred to as ppt-*ACE2*. Lentiviral particles expressing ACE2 were produced by co-transfecting ppt-*ACE2*, a 2nd generation lentiviral packaging construct psPAX2 and VSV-G plasmid pMD2.G (Addgene #12259) in HEK293T cells by using polyethylenimine as previously described[55]. Virus supernatant was harvested 72 hours post transfection, pre-cleared of cellular debris and centrifuged at 28,000 xg for 90 minutes at 4 °C to generate concentrated virus stocks. To transduce HEK293T cells, 10,000 cells per well were seeded in a 96 well tissue culture plate and virus supernatant added in a 2-fold dilution series. At 72 hours post transduction the surface expression of ACE2 was measured by immunostaining the cells with anti-ACE2 monoclonal antibody (Thermo Fisher Scientific, MA5-32307). Cells showing maximal expression of ACE2 were then sorted into single cells using BD FACS Aria III cell sorter to generate clonal populations of HEK293T-*ACE2* cells.

For generating HEK293T cells expressing both ACE2 and TMPRSS2 (HEK293T-*ACE2-TMPRSS2*), HEK293T-*ACE2* cells described above were transduced with lentiviral particles expressing *TMPRSS2*. To achieve this, *hTMPRSS2a* (synthetic gene fragment; IDT) was cloned into lentiviral expression vector pLVX-IRES-ZsGreen (Clontech) using EcoR1/XhoI restriction sites and lentiviral particles expressing *TMPRSS2* were produced as described above. Lentiviral transductions were then performed on HEK293T-*ACE2* cells to generate HEK293T-*ACE2-TMPRSS2* cells. Clonal selection led to the identification of a highly permissive clone, HekAT24[53], which was then used in subsequent experiments.

512

513 **Optimizing a flow cytometry-based assay for determining SARS-CoV-2 Spike binding**

514 HEK293T-*ACE2* cells were dissociated by incubating with TrypLE for 5 min at 37°C and
515 neutralized with DMEM. 10^6 cells were collected, washed with 1% bovine serum albumin (BSA;
516 Sigma-Aldrich) in Dulbecco's Phosphate Buffered Saline (DPBS; Sigma-Aldrich) and then
517 incubated with increasing concentrations of Alexa Fluor 488-conjugated SARS-CoV-2 spike
518 glycoprotein (Spike488) for 30 min at 4°C. The cells were then washed once with DPBS before
519 resuspending in 1% BSA in DPBS and analyzed using the Cytek Aurora (Cytek Biosciences). For
520 cell mixing experiments, increasing proportions of HEK293T-*ACE2* cells (0%, 1%, 20%, 50%,
521 80% and 100%) were combined with decreasing proportions of wildtype (WT) HEK293T cells
522 (100%, 99%, 80%, 50%, 20%, 0%) to a total of 10^6 cells per sample. These samples were incubated
523 with 50 μg/mL Spike488 as described above and analyzed using the Cytek Aurora (Cytek
524 Biosciences).
525 To confirm the validity of this assay in detecting binding in cells expressing CRISPRa machinery,
526 a clonal line of HEK293T with stable expression of a plasmid encoding dCas9-VP64 and SAM
527 system helper proteins (pPB-R1R2_EF1aVP64dCas9VP64_T2A_MS2p65HSF1-IRESbsdpA)
528 (HEK293T-CRISPRa) was transduced with lentivirus carrying *ACE2* sgRNA 1 or non-targeting
529 control sgRNA. These cells were then incubated with Spike488 as previously described and
530 analyzed on the Cytek Aurora (Cytek Biosciences).

531

532 **CRISPR activation screening**

533 HEK293T-CRISPRa cells were transduced with concentrated Human CRISPR activation pooled
534 library set A (Addgene #92379)-carrying lentivirus at a multiplicity of infection (MOI) of

535 approximately 0.3. Cells were selected on puromycin dihydrochloride (Gibco) at a concentration
536 of 1.6 µg/mL for 3 days (screen 1 and 2). $3x10^7$ cells (>500 cells/guide) were incubated with
537 Spike488 for 30 min at 4°C, washed to remove excess spike protein, and sorted for increased Alexa
538 Fluor 488 intensity using the BD FACSMelody Cell Sorter (BD Biosciences). Gates for flow
539 assisted cytometric sorting were set using non-targeting control (NTC) sgRNA-transduced cells as
540 a negative control and *ACE2* sgRNA-transduced cells as a positive control, both of which had been
541 incubated with Spike488 under the same conditions as stated previously. Unsorted cells were
542 maintained separately so as to be used as a diversity control. Cells were expanded and $1.5\text{-}2x10^6$
543 cells were then collected for genomic DNA (gDNA) extraction for sorted samples and $3x10^7$ for
544 the unsorted diversity control. Remaining diversity control cells were re-seeded and once again
545 incubated with Spike488 under the same conditions as stated previously (screen 3). These Spike-
546 incubated cells were sorted again but selected on puromycin for eight days prior to expansion and
547 collection of $1x10^7$ cells from both the sorted cell population and the unsorted diversity control
548 population for gDNA extraction. Gating strategy is shown in **Supplementary Fig. 1b**.
549
550 gDNA was extracted from all collected cells using the ISOLATE II Genomic DNA Kit (Bioline).
551 Samples were prepared for NGS via PCR. Genomic DNA (25 µg for unsorted diversity control
552 samples, 5 µg for sorted samples) was added to NEBNext High-Fidelity 2X PCR Master Mix (New
553 England Biolabs) and 0.4 µM P5 staggered primer mix and 0.4 µM of P7 indexing primer unique
554 to each sample. PCR cycling conditions and primers were adapted from Sanson et al.[5]. Primer
555 sequences can be found in **Supplementary Table 3**. Briefly, reactions were held at 95°C for 1
556 min, followed by 28 cycles of 94°C for 30 s, 53°C for 30 s and 72°C for 30 s, followed by a final
557 72°C extension step for 10 min. Amplicons were gel extracted and purified using the ISOLATE II

PCR & Gel Kit (Bioline) and the quality and concentration of DNA assessed with the High Sensitivity DNA kit (Agilent Technologies). Samples were then sent to Novogene for next generation sequencing. Raw next generation sequencing reads were then processed using MAGeCK (v0.5.9.2)[7] to identify enriched genes. Median normalization was used with gene test FDR threshold set to 0.1. Plots were generated using MAGeCKFlute (v1.12.0)[8] Normalized read counts were produced using MAGeCK 'count' function on each pairing of unsorted diversity control and sorted sample. Mean and standard deviation was calculated for each individual sample (i.e. separately for diversity control and sorted sample) and the Z-score calculated using $Z = \frac{x - \mu}{\sigma}$, where x is the normalized read count for an individual sgRNA, μ is the mean of all normalized read counts in the sample and σ is the standard deviation of all normalized read counts in the sample.

Validation of ACE2 and LRRC15 by CRISPRa

To validate the function of LRRC15 in binding SARS-CoV-2 spike, clonal HEK293T-CRISPRa cells were transduced with lentivirus carrying *ACE2* sgRNAs, *LRRC15* sgRNAs or a NTC sgRNA. Cells were selected on 1.6 µg/mL puromycin dihydrochloride (Gibco) for 3 days and then collected for analysis by RT-qPCR and flow cytometry. For validation by flow cytometry, $1x10^6$ cells were incubated with 50 μg/mL Spike647 as previously described and then analyzed using the Cytek Aurora (Cytek Biosciences). Binding affinity of ACE2 and LRRC15 were conducted with *ACE2* sgRNA3 and *LRRC15* sgRNA1 cells with 1, 5, 10, 25, 50 and 100 μg/mL Spike647 (corresponding to 7, 35, 70, 175, 350 and 700 nM) .

RNA extraction and RT-qPCR

RNA was isolated from cells using the ISOLATE II RNA Mini Kit (Bioline) and concentration was measured by Nanodrop (Thermo Scientific). cDNA was synthesized using the iScript Select cDNA Synthesis Kit (Bio-Rad) according to manufacturer's instructions. Briefly, 50-500 ng of RNA was added to iScript RT Supermix and nuclease-free water to a final volume of 10 µL. The assembled reactions were then incubated in a thermocycler as follows: 25°C for 5 min, 46°C for 20 min and then 95°C for 1 min. RT-qPCR was then performed on the cDNA samples using SYBR Select Master Mix (ThermoFisher Scientific) and the LightCycler 480 System (Roche). All primer sequences used are listed in **Supplementary Table 4**. Results were analyzed using the $\Delta\Delta C_T$ method.

LRRC15 crystal structure prediction

The predicted crystal structure for LRRC15 was calculated using AlphaFold (v2.0)[56] (https://alphafold.ebi.ac.uk/entry/Q8TF66) and sourced via UniProt[57] (https://www.uniprot.org/uniprot/Q8TF66).

LRR Tollkin Phylogenetic Tree

Protein sequences of LRR Tollkin family members[12] were clustered using Clustal Omega (v1.2.2)[58]. The phylogenetic (Newick) tree was visualized with MEGA11[58,59].

Validation of LRRC15 independent of CRISPR activation

LRRC15-TurboGFP fusion constructs (Origene, RG225990 and RG221437) were used for flow cytometry, immunoprecipitation and immunocytochemistry experiments while *LRRC15-myc-DDK* fusion constructs (Origene, RC225990 and RC221437) were utilized for SARS-CoV-2

604 authentic virus inhibition experiments. Both *TurboGFP*-tagged and *Myc-DDK*-tagged *LRRC15*
605 constructs were used in pseudovirus infection experiments assessing *cis*-inhibition of infection.
606 *LRRC15* transcripts were excised from the *LRRC15-TurboGFP* and *LRRC15-myc-DDK* constructs
607 and replaced with multiple cloning sites to generate empty vector controls for transfection.
608
609 To evaluate the role of LRRC15 in binding SARS-CoV-2 spike glycoprotein independent of
610 CRISPR activation machinery, 2.5 µg of plasmids carrying the *GFP*-tagged *LRRC15* cDNA
611 transcript 1 or 2, or empty vector control (pLJM1-EGFP; Addgene #19319) were transfected into
612 HEK293T, HEK293T-*ACE2* and HEK293T-*ACE2-TMPRSS2* cells as described above. For each
613 sample, 10^6 cells were collected and incubated with Alexa Fluor 647-conjugated SARS-CoV-2
614 spike glycoprotein (Spike647) and analyzed using the Cytek Aurora (Cytek Biosciences) as
615 described above.
616
617 **Immunoprecipitation**
618 For SARS-CoV-2 spike pulldown, $2x10^7$ HEK293T cells transfected with *LRRC15-TurboGFP*
619 (transcript 1 and 2) or *pLJM1-EGFP* (Addgene #19319) were incubated with 50 µg/mL spike
620 hexapro for 30 min at 4°C with rotation. Cells were washed with DPBS (Sigma-Aldrich, D8537)
621 and incubated for 15 min in lysis buffer (1% Igepal-CA-630, 5 mM Tris HCl (pH 7.4), 150 mM
622 NaCl, 1 mM $MgCl_2$, 5% glycerol, 10 mM NaF, 10 mM sodium pyrophosphate, 10 mM sodium
623 orthovanadate, 60 mM β-Glycerophosphate, 1X complete EDTA-free protease inhibitor (Roche))
624 on ice. Samples were then sonicated at 90% amplitude for 30 seconds using the BANDELIN
625 SONOPULS mini20 and spun down at 18,000 g for 10 mins. Concentration of protein samples
626 was determined using BCA assay (ThermoFisher Scientific). 1 µg of anti-LRRC15 antibody

(Abcam, EPR8188(2)) or rabbit IgG (Covance, CTL-4112) was added to 1 mg protein lysate and incubated at 4°C with rotation for 2.5 h before precipitation with protein G (ThermoFisher Scientific). Immunoprecipitated proteins were eluted with 0.1 M Tris and 4% SDC. Input, flow-through and eluate were mixed with 4X loading buffer and heated at 95°C for 5 min. Samples were loaded into pre-cast polyacrylamide gels (4-20% gradient, Bio-Rad) and electrophoresed at 90 V for 1.5 h. Proteins were transferred to 0.45 µm nitrocellulose membranes at 100 V for 1 h. Membranes were blocked in Intercept blocking buffer (LI-COR) for 30 min at room temperature with gentle agitation. Blocking solution was replaced with primary antibody (Spike, LRRC15) Intercept buffer and membranes incubated overnight at 4°C with gentle agitation. Membranes were washed three times with TBST for 5 min with agitation prior to the incubation of membranes with secondary antibody in Intercept buffer for 2 h at room temperature. Membranes were washed another three times with TBST and then imaged using the Odyssey CLx (LICOR).

Confocal imaging of cultured cells

13 mm round coverslips were coated with Matrigel (Corning) diluted in DPBS and incubated for 30 min at 37°C. HEK293T cells transfected with *LRRC15* cDNA constructs were seeded onto the Matrigel-coated coverslips at a density of 50,000 cells per coverslip. The following day, cells were incubated with Alexa Fluor™ 647-conjugated SARS-CoV-2 spike protein at a concentration of 10 µg/mL in culture media for 30 min at 37°C. The cells were fixed in 4% paraformaldehyde (PFA) for 20 min at room temperature, washed 3 times with DPBS. Cells were incubated with Hoechst (1:2000 in DPBS) for 20 minutes, washed 3 times and mounted onto Superfrost plus slides (Fisherbrand) and then imaged using the Leica TCS SP8 STED 3X at 40X magnification.

650 **Patients**

651 Post-mortem formalin-fixed paraffin embedded (FFPE) tissue samples were obtained from 4
652 patients who died from severe COVID-19 infection and diagnosed using a PCR test between
653 December 2020 and March 2021. The control group consisted of post-mortem FFPE lung tissue
654 samples from 3 patients with melanoma metastases in the lung. Lung tissue from COVID-19
655 patients was compared with non-tumor lung tissue from melanoma patients. All patients gave
656 informed consent for study participation and the study was performed in accordance with the
657 Declaration of Helsinki guidelines. The study was approved by the Ethics Committee of Eastern
658 Switzerland (BASEC Nr. 2020-01006/EKOS 20/71 and BASEC Nr. 2016-00998/EKOS 16/015).
659

660 **Hematoxylin and Eosin (H&E) staining, LRRC15 and collagen I immunofluorescence (IF)**

661 Post-mortem lung tissue samples were collected and processed for paraffin embedding according
662 to standard diagnostic protocols in the Institute for Pathology of St. Gallen Cantonal Hospital. All
663 tissue samples were routinely stained for histopathological diagnosis with H&E following a
664 standardized validated protocol. Two-micron-thick sections were cut using a Leica RM2255 rotary
665 microtome (Leica Microsystems, DE) and placed on poly-L-lysine-coated slides. Slides were
666 dewaxed in xylene, rehydrated, and subjected to heat-induced epitope retrieval in a sodium citrate
667 solution (pH 6) for 20 minutes in a microwave oven. Slides were then allowed to cool to room
668 temperature followed by a 60-minute incubation with 1x PBS/5% skim milk at RT. Excess liquid
669 was removed and sections were incubated for 18 h at 4°C with a polyclonal rabbit anti-human
670 LRRC15 antibody (LSBio, catalog number LS-C405127, lot ID 134873, dilution 1:50) in 1x PBS.
671 This step was followed by a 1 h incubation at RT with an Alexa Fluor 488 donkey anti-rabbit IgG
672 (H+L) antibody (Jackson Immunoresearch, catalog number 711-545-152, dilution 1:200) in 1x

PBS, and another incubation for 2 h at RT with a monoclonal mouse anti-human collagen I antibody (Abcam, catalog number ab88147, clone 3G3, dilution 1:100) labelled with an Alexa Fluor 647 antibody labeling kit (Invitrogen, catalog number A20186) following the manufacturer's instructions. Slides were then counterstained with DAPI, and mounted using fluorescence mounting medium (Dako, Cat. No. S3023).

Image acquisition for stained lung tissue samples

Whole slide scans of H&E-stained slides were acquired with a Pannoramic 250 Flash III digital slide scanner (3D Histech, HU). All micrographs from the IF stain were acquired using an LSM980 confocal microscope with Airyscan 2 (Zeiss, DE).

Generation of TurboGFP-only and TurboGFP-tagged LRRC15 cDNA overexpression lines

VELOCITY DNA Polymerase was used in PCR to generate amplicons containing cDNA for *TurboGFP*-tagged *LRRC15* Transcript 1 (from Origene plasmid RG225990) and *TurboGFP* control. PCR was similarly used to amplify all components from the LentiCRISPR-v2 plasmid with the exception of the *U6-sgRNA* sequence and *Cas9* protein coding sequence. NEBuilder HiFi DNA Assembly Master Mix was used to assemble lentiviral *LRRC15-TurboGFP* and *TurboGFP*-only cDNA constructs using the cDNA amplicons as inserts and LentiCRISPR-v2 fragment as the vector backbone. Assembly products were transformed into 10-beta cells via heat shock, plated onto agarose containing ampicillin at a concentration of 100 µg/mL and incubated for approx. 16 h at 37°C. Individual colonies were picked, expanded in Luria broth (Life Technologies) supplemented with ampicillin and amplified constructs were harvested using ISOLATE II Plasmid Mini Kit (Bioline). Successful construct assembly was confirmed via Sanger Sequencing.

Lentivirus production and transduction of IMR90 fibroblasts and HEK293T-*ACE2-TMPRSS2* cells was carried out as previously described. Cells were then selected on puromycin at a concentration of 2 μg/mL for a minimum of 72 h and functional cDNA expression confirmed by observation of fluorescence.

SARS-CoV-2 pseudotyped lentivirus production and infection assay

SARS-CoV-2 pseudovirus was produced using a five-component plasmid system. Plasmid encoding the SARS-CoV-2 spike protein with an 18 amino acid truncation of the C-terminus or the Delta variant of the SARS-CoV-2 Spike protein was co-transfected into HEK293T cells with pBCKS(HIV-1SDmCMBeGFP-P2A-luc2pre-IIU), which permits equimolar expression of firefly luciferase and EGFP, and packaging plasmids pHCMVgagpolmllstwhv, pcDNA3.1tat101ml and pHCMVRevmlwhvpre. Transfection was carried out using Lipofectamine 3000 Transfection Reagent (ThermoScientific) according to manufacturer's instructions. 16 h after transfection, a media change was performed. Viral media was collected the following day, passed through a 0.45 μm filter and then concentrated using 100K MWCO Pierce Protein Concentrators (Life Technologies Australia). Concentrated virus was then stored at -80°C. Pseudovirus particle concentrations were determined using the QuickTiter™ Lentivirus Titer Kit (Cell Biolabs, Inc) under manufacturer conditions.

For infection of cells with SARS-CoV-2 pseudovirus in *cis* inhibition assays, WT HEK293T, HEK293T-*ACE2* and HEK293T-*ACE2-TMPRSS2* cells were transfected with cDNA for *myc-DDK*-tagged *LRRC15* transcript 1 or a control plasmid (lentiGuide-Puro; Addgene #52963). Cells were seeded in 96-well plates, concentrated pseudovirus was added 24 hours later in the presence

719 of 8 µg/ml Polybrene. Successful transduction of cells was confirmed by observing GFP
720 expression 48 h post-tranduction. The extent of transduction was quantified with the Steady-Glo
721 Luciferase Assay System (Promega Corporation) according to the manufacturer's instructions.
722 Briefly, plates were allowed to equilibrate to room temperature before 50 µL of Steady-Glo reagent
723 was added to each well containing 50µL of cell culture media. Plates were incubated at room
724 temperature for 1 h to permit cell lysis and luminescence was then measured using a plate reader.
725 Luminescence of the *LRRC15* cDNA- and control plasmid-transfected cells was normalized to the
726 luminescence values for control cells infected at corresponding viral concentration / pseudovirus
727 number.
728
729 **SARS-CoV-2 authentic virus infection assays**
730 For assessing the inhibitory effect of native overexpression of LRRC15, HEK293T-*ACE2-*
731 *TMPRSS2* cells were transfected with *myc-DDK*-tagged *LRRC15* transcript 1 plasmid (Origene,
732 RC225990) for transient overexpression, with empty *myc-DDK* plasmid as a control plasmid.
733 HEK293T-*ACE2-TMPRSS2* cells were seeded in 384-well plates at a density of 8×10^3 cells/well
734 in the presence of NucBlue™ live nuclear dye (Invitrogen, USA) at a final concentration of 2.5%
735 v/v. The SARS-CoV-2 isolates (Wuhan) were serially diluted in cell-culture medium and an equal
736 volume was then added to the pre-plated and nuclear-stained cells to obtain the desired MOI doses.
737 Viral dilutions were performed in duplicate. Plates were then incubated at 37°C for 48 hours before
738 whole wells were imaged with an IN Cell Analyzer HS2500 high-content microscopy system
739 (Cytiva). Nuclei counts were obtained with automated IN Carta Image Analysis Software (Cytiva)
740 to determine the percentage of surviving cells compared to uninfected controls. *LRRC15* and

control plasmid-transfected cells were normalized to the average cell count of uninfected wells for the corresponding cell type to determine the extent of normalized cell death.

Single cell RNA-sequencing analysis

LRRC15 expression was first queried on the COVID-19 cell atlas interactive website and summarized in **Fig. 5a**. In depth analysis of lung single cell datasets were conducted on 3 studies[24–26] with Seurat V4.1.0[60]. Two single nucleus RNAseq datasets were downloaded from the Single Cell Portal (Broad Institute, SCP1052 and SCP1219) and one single cell RNAseq dataset from Gene Expression Omnibus (GSE158127). Their accompanying metadata, which includes information such as sample ID, sample status and cluster annotations (cell types), were added to Seurat objects using the 'AddMetaData' function. Read counts were normalized using SCTransform, before reanalysis with the standard Seurat workflow of 'RunPCA,' 'FindNeighbours,' 'FindClusters,' and 'RunUMAP'. Cluster identities were assigned using published cluster annotations and plots were generated with 'DimPlot' and 'DotPlot'. The number of cells in each cluster from each study was then tabulated. 'Subset' was utilized to create new fibroblast only datasets before generating collagen (*COL1A1*, *COL1A2*, *COL8A1*, *COL11A1*, *COL12A1*) dotplots for *LRRC15*-expressing (*LRRC15*>0, Pos) and non-expressing (*LRRC15* = 0, Neg) fibroblasts.

Fibroblast infectivity and SARS-CoV-2 pseudovirus co-culture assay

LRRC15 expression in IMR90 lung fibroblasts were first compared with HEK293T cells by RT-qPCR. These cells were then transfected with empty *TurboGFP* control and *LRRC15-TurboGFP* (Lipofectamine LTX with plus reagent (ThermoScientific)). Cells were checked for Spike binding

764 activity by incubation with Spike647 and detection via flow cytometry 24 h post-transduction.
765 Then, these fibroblasts were infected with SARS-CoV-2 pseudovirus as described above and
766 luciferase luminescence were compared to HEK293T-*ACE2-TMPRSS2* cells.
767
768 For SARS-CoV-2 pseudovirus co-culture assay, IMR90 fibroblasts stably over-expressing either
769 *TurboGFP*-alone or *TurboGFP*-tagged *LRRC15* Transcript 1 were mixed with HEK293T-*ACE2-*
770 *TMPRSS2* in a ratio of 2:1 and then seeded at a density of 18,000 cells per well in 96-well plates.
771 SARS-CoV-2 pseudovirus was added to cells the following day in fresh media containing 8 ug/mL
772 Polybrene. Extent of transduction was quantified approximately 16 h later using the Steady-Glo
773 Luciferase Assay System (Promega Corporation) as previously described.
774
775 **Authentic SARS-CoV-2 Virus Bioassay of co-cultured cells**
776 For assessing virus infectivity in the presence of native LRRC15 over-expression, co-culture
777 conditions were established by mixing IMR90 fibroblasts that stably over-expressed *TurboGFP-*
778 tagged *LRRC15* transcript 1 or *TurboGFP*-only with HEK293T-*ACE2-TMPRSS2* at a ratio of 2:1.
779 The cell suspensions were seeded on 96-well plates at a density of 18000 cells per well. SARS-
780 CoV-2 isolates (Wuhan) were serially diluted in culture medium and an equal volume was added
781 to seeded cells. Plates were incubated for 24 h at 37℃, and the media was collected and diluted
782 1:10. This media was added using equal volumes in an infection bioassay consisting of
783 hyperpermissive HEK293T-*ACE2-TMPRSS2* cells that were seeded in 384-well plates (3000
784 cells/well). Plates were incubated for 72 h at 37℃, and NucBlueTM live nuclear dye (Invitrogen,
785 USA) at a final concentration of 2.5% was added. After a 4 h incubation plates were imaged using
786 an IN Cell Analyzer HS2500 high-content microscopy system (Cytiva). Quantification of nuclei

was performed with automated IN Carta Image Analysis Software and normalised to uninfected wells.

RNA Sequencing

Total RNA was extracted from IMR90 fibroblasts overexpressing *TurboGFP* alone or *TurboGFP*-tagged *LRRC15* Transcript 1 using the ISOLATE II RNA Mini Kit (Bioline) and quantified via Qubit. 200 ng of each sample was processed with the Illumina Stranded mRNA Prep kit and indexes added with the IDT for Illumina RNA UD Indexes Set A. The prepared libraries were quantified via Qubit and then pooled at a final concentration of 750 pM. PhiX was spiked in at 2% and the pooled libraries were then sequenced on the Illumina NextSeq 2000.

Differential Gene Expression Analysis and Ingenuity Pathway Analysis

Differential gene expression analysis was performed using Illumina BaseSpace. Briefly, the BCL Convert app (v2.1.0) was used to generate fastq files from the sequencing run. The DRAGEN FASTQ Toolkit app (v1.0.0) was used to trim adapter sequences and the 5' T-overhang generated during adapter ligation. DRAGEN FastQC + MultiQC (v3.9.5) was used for quality control checks. DRAGEN RNA (v3.10.4) was used for read counting with hg38 Alt-Masked v2, Graph Enabled used as the reference genome. Finally, DRAGEN Differential Expression (v3.10.5) was used for differential gene expression analysis. Output can be found in **Supplementary Table 5**. Output of this differential gene expression analysis was uploaded to Ingenuity (v01-21-03) and filtered such that only genes with adjusted p-value < 0.05 were used in core analysis. Canonical pathway analysis output can be found in **Supplementary Table 6.** Canonical pathways that had a Z-score of 0 or no activity pattern available were disregarded.

Quantification and statistical analysis

SARS-CoV-2 spike glycoprotein titration experiments were analyzed on GraphPad Prism and fitted with non-linear regression (one site -- specific binding) to identify maximal binding (B_{max}) and dissociation constants (K_D). CRISPR activation screen analysis was performed using MAGeCK (v0.5.9.2)[7]. For each sample, Z-scores were calculated using normalized read counts. Volcano plots were generated using the EnhancedVolcano package for R. All other plots were generated using ggplot2 or GraphPad Prism. All flow cytometry data was analyzed using FlowJo. All RT-qPCR results were analysed using $\Delta\Delta C_T$ method. For *LRRC15* and *COL1A1* RT-qPCR in TGFβ-treated cells, *LRRC15* and *COL1A1* expression in each sample was normalised to expression in untreated cells. Significance was assessed with Mann-Whitney One Tailed t-test. For SARS-CoV-2 pseudovirus and live virus experiments, data shown reflects ≥3 independent replicates. For pseudovirus experiments in monocultures, results are reported as either raw luminescence values or as normalized level of transduction, calculated by dividing luminescence recorded for LRRC15-transfected cells by luminescence relative to control. For pseudovirus co-culture experiments, normalized level of transduction was calculated by dividing luminescence recorded for LRRC15 expressing cells by control cells transduced at the same number of pseudovirus particles. For authentic virus monoculture and co-culture infection assays, cell death for both control and LRRC15-transfected cells was normalized to uninfected cells of the same line. Significance for SARS-CoV-2 pseudotyped lentivirus and authentic virus experiments were analyzed with two-way ANOVA with Sidak Multiple Comparisons test. For analysis of pooled independent single cell/nuc sequencing datasets, significance was assessed using unpaired t-test. Significance of differentially expressed genes was assessed using the DRAGEN Differential

Expression application, which utilizes DESeq2. Z-score for DEG canonical pathways was determined by Ingenuity. For RT-qPCR confirmation of upregulated antiviral gene signature and downregulated collagen gene signature, expression was normalized to the average of the control GFP cells and significance was assessed using One-Tailed Mann-Whitney tests. All error bars in this manuscript report SEM unless otherwise stated.

Acknowledgements

We thank Novogene for CRISPRa library sequencing, Sydney Informatics Hub (Artemis HPC) for single cell data analysis infrastructure, Sydney Cytometry for flow cytometry and FACS support, the technical and scientific assistance of Sydney Microscopy & Microanalysis, the University of Sydney node of Microscopy Australia, Dr Megan Steain, Dr Mark Larance, Dr Sean Humphrey, Dr Gang Liu, Dr Phil Hansboro, Dr Tim Newsome and members of the Neely lab for helpful discussions. Figure illustrations were created with BioRender.com.

Funding

G.N. is funded by the National Health and Medical Research Council (NHMRC) project grants APP1107514, APP1158164, APP1158165, the NSW Ministry of Health, and a philanthropic donation from Dr. John and Anne Chong. L.L. is funded by a Dr. John and Anne Chong Fellowship for Genome Editing and seed funding from the Drug Discovery Initiative at the University of Sydney. L.F. is supported by the Swiss National Science foundation grant PP00P3_157448. O.H.A. is funded by a Swiss National Science Foundation fellowship no. P400PM_194473..

Author contributions

LL, GGN conceived this project. LL, FC established the CRISPRa system. MW validated the efficiency of the CRISPRa system. LL, MW performed whole genome screening and target validation. LL, AJC performed pseudolentivirus *Cis* experiments with input from DH. CLM performed microscopy of cultured cells. LL performed western blots. AJ, OHA, and OTP designed, performed, and analysed human lung histology. MW, CED performed molecular cloning. AA generated ACE2 and ACE2-TMPRSS2 cell lines. MW generated stable overexpression lines and carried out RNA sequencing analysis. MW, ZH performed RT-qPCR. JKKL, KP, RS, JM produced Spike protein. CLM, ST, AJC, DH, TK, and SM helped with SARS-CoV-2 neutralization studies. LL, MW, AJC, CLM, AOS, DH, GGN performed data analyses. LL, LF, DH, ST, GGN provided supervision and project administration. LL, MW, GGN wrote the manuscript with contributions from all authors.

Declaration of interests

The authors declare no competing interests.

Figure Legends

Figure 1. A sensitive FACS-based SARS-CoV-2 Spike binding assay amenable to high throughput screening.

a Schematic of SARS-CoV-2 Spike binding assay. HEK293T cells with stable integration of *ACE2* cDNA for overexpression (HEK293T-*ACE2*) are incubated with Alexa Fluor 488-conjugated SARS-CoV-2 Spike protein (Spike488). Spike488-binding cells are then detected by flow cytometry. **b** Representative flow cytometry plots for *WT* HEK293T and HEK293T-*ACE2* incubated with Spike488 (N=3). See also **Supplementary Fig. 1b** for gating strategy. **c** Titration of HEK293T-*ACE2* (*ACE2*) cells with *WT* HEK293T cells. 1% HEK293T-*ACE2* cells showed a difference to baseline non-specific binding. Histogram summary showing mean fluorescence intensity (MFI) of flowed cells. **d** Schematic of CRISPR activation (CRISPRa) system used. **e** Representative plot of flow cytometry for a clonal HEK293T-CRISPRa cell line transduced with NTC sgRNA or *ACE2* sgRNA (expression confirmation via RT-qPCR in **Supplementary Fig. 1a**).

Figure 2. Whole genome CRISPRa screening identified LRRC15 as a novel SARS-CoV-2 Spike-binding protein.

a Schematic of CRISPRa screen used to identify regulators of SARS-CoV-2 Spike-binding. **b** Ranking of all genes in screen 1 by $\log_2$ fold change calculated using MAGeCK and plotted using MAGeCKFlute. See also **Supplementary Table 1**. **c** Gene enrichment analysis of screen 1 performed using MAGeCK. Horizontal dotted line indicates p-value = 0.05. Vertical dotted line indicates $\log_2$ fold changes (LFCs) of 2. P-values and LFCs for all genes are reported in

Supplementary Table 1. **d** sgRNA Z-scores for screen 1 unsorted and sorted samples. Density curve for all sgRNA Z-scores in sample (i.e. sorted or unsorted) is shown in grey. Z-scores for each guide are indicated by vertical lines (blue ACE2, red LRRC15). **e** Flow cytometry analysis of HEK293T-CRISPRa cells transduced with three independent *LRRC15* sgRNAs. HEK293T-CRISPRa transduced with *ACE2* sgRNA3 were used as a positive control and NTC sgRNA-transduced HEK293T-CRISPRa cells were used as a negative control (N = 3). **f** Quantification of Spike647 binding in *ACE2* sgRNA3 and *LRRC15* sgRNA1 cells via flow cytometry. Dissociation constant (Kd) was calculated by fitting with non-linear regression (one site -- specific binding). N = 3, error bars represent S.D.

Figure 3. Confirmation that LRRC15 binds to SARS-CoV-2 Spike protein.

a LRRC15 contains 15 leucine-rich repeats, a short cytoplasmic C-terminus, and 2 glycosylation sites. **b** Predicted protein structure of LRRC15 (from alpha fold). **c** LRRC15 is part of the LRR-Tollkin family. **d** Flow cytometry analysis of Alexa Fluor-647 (Spike647) binding in WT HEK293T cells, **e** HEK293T-*ACE2* and **f** HEK293T cells with stable expression of *ACE2* cDNA and *TMPRSS2* cDNA (HEK293T-*ACE2*-*TMPRSS2*). Each cell line was transfected with plasmids encoding cDNA for *GFP*-tagged *LRRC15* (transcript 1 or 2) or with empty *GFP* vector as negative control plasmid. **g**. Histogram summary shows mean fluorescence intensity (MFI) of **d-f**. **h** Representative images of interaction between LRRC15-GFP and Alexa Fluor 647-conjugated SARS-CoV-2 HexaPro Spike protein in HEK293T cells (N = 2). Images were taken at 40x magnification. Green = LRRC15-GFP, Red = Spike647, Blue = Hoechst-stained nuclei. Scale bar = 25 μm. **i** Immunoprecipitation of LRRC15 with Spike protein. Lysates of HEK293T cells transfected with GFP-tagged *LRRC15* (transcript 1 or 2, *LRRC15_1* and *LRRC15_2*, respectively)

incubated with SARS-CoV-2 HexaPro Spike protein were immunoprecipitated using anti-LRRC15 primary antibody. Immunoblots were performed for LRRC15 and for SARS-CoV-2 HexaPro spike. I = input, FT = flow-through, E = elute.

Figure 4. LRRC15 is expressed in lung fibroblasts and lines the airways in COVID-19 patients.

a Overview of cell types expressing *LRRC15* from existing single cell RNA-sequencing datasets. **b** UMAP plot of lung single nucleus RNAseq dataset (Melms et al). **c** Feature plot and **d** Dotplot shows *LRRC15* is expressed in fibroblasts and neuronal cells. Expression of *LRRC15* is also observed in fibroblasts of separate studies (See **Supplementary Fig. 5**). **e** Proportion of cells that are lung fibroblasts increases with COVID lungs (7.9% in control (N = 19) and 22.9% in COVID (N = 47); Unpaired t test, $p<0.0001$) **f-g** Representative micrograph of hematoxylin and eosin (H&E) stained lung tissue section obtained from **f** a human donor without COVID-19 and **g** donor diagnosed with COVID-19. Imaging performed at 200x magnification (Scale bar = 50 m). All images in **Supplementary Fig. 6a** (Control, N = 1; COVID-19, N = 4). **h-i** Representative micrograph of immunofluorescence staining in human lung tissue section obtained from **h** donor without COVID-19 and **i** donor diagnosed with COVID-19. Images were taken at 200x magnification (Scale bar = 100 m). Red = Collagen I, green = LRRC15, blue = DAPI. All images in **Supplementary Fig. 6b** (Control, N = 3; COVID-19, N = 4).

Figure 5. LRRC15 is not a SARS-CoV-2 entry receptor but inhibits infection in *trans*.

a IMR90 fibroblasts express *LRRC15*, quantified via RT-qPCR. N=3 per cell line. **b-c** TGFβ increased **b** *LRRC15* and **c** *COL1A1* in fibroblasts, quantified via RT-qPCR. N = 7 for each group.

Significance was determined by Mann-Whitney One-Tailed test, **p<0.01. **d** IMR90 fibroblasts expressing *LRRC15* bind spike, MFI = Mean Fluorescence Intensity. **e** Fibroblasts do not have innate tropism for SARS-CoV-2 and overexpression of *LRRC15* does not mediate infection. Transduction efficiency (luciferase luminescence) was compared to permissive cell line HEK293T-*ACE2-TMPRSS2*. N = 2 independent replicates for each group. **f** Pooled analysis of 3 independent studies indicate ratio of fibroblasts to epithelial cells in COVID lungs is approx. 2:1 (0.3 in control (n=19) and 2.06 in COVID (n=47); Unpaired two-tailed t test, p<0.0001). **g** LRRC15 expressing fibroblasts can suppress SARS-CoV-2 spike pseudovirus infection of HEK293T-*ACE2-TMPRSS2* cells. Significance was determined by two-way ANOVA, Sidak's multiple comparison test, **p<0.01,*p<0.05. N = 6 per condition. **h** LRRC15 expressing fibroblasts can suppress authentic SARS-CoV-2 infection of HEK293T-*ACE2-TMPRSS2* cells. Significance was determined by two-way ANOVA, Sidak's multiple comparison test, *p<0.05. N = 3 per condition.

Figure 6. LRRC15 expression is correlated with collagen and antiviral gene signatures.

a *LRRC15*$^{+}$ fibroblasts have an enhanced collagen gene signature. Dotplots generated from 3 separate studies. Pos = *LRRC15*$^{+}$, Neg = *LRRC15*$^{-}$. **b** Volcano plot of differentially expressed genes (DEGs) from fibroblasts ectopically expressing either LRRC15 or GFP. N = 3 biological replicates for each group. A subset of DEGs is labelled, including collagen genes and genes related to antiviral signaling. Blue labels indicate downregulation while red labels indicate upregulation. **c** DEG-associated canonical pathways as determined by Ingenuity Pathway Analysis. Canonical pathways were filtered to show only those with p-value < 0.05 and with a nonzero Z-score (i.e., pathways that had no activity pattern or a Z-score of 0 are not shown). **d-e** *LRRC15* overexpression

causes **d** upregulation of antiviral transcripts and **e** downregulation of collagen transcripts by RT-qPCR. Results were calculated using the $\Delta\Delta C_T$ method, normalized to the average of control *GFP*-only cells. Significance was assessed using one-tailed Mann Whitney test, *p<0.05. N = 3 per condition. **f** Ectopic expression of LRRC15 in fibroblasts decreases Collagen VI protein expression compared to *GFP*-only control cells. Western blots for LRRC15 and Collagen VI.

Supplementary Fig. 1. CRISPR activation screen setup.

a RT-qPCR of *ACE2* expression in SAM clonal cell lines transduced with *ACE2* sgRNAs, or with HEK293T-*ACE2* cells. Results calculated using $\Delta\Delta C_T$ method and normalized to non-targeting control (NTC) sgRNA-transduced HEK293T-CRISPRa cells. **b** FACS gating strategy. Cells were first gated by forward (FSC) and side scatter (SSC) before filtering for singlets. Spike488 fluorescence was gated by comparison with non-targeting control (NTC) sgRNA transduced cells. Similar strategy was applied to all flow cytometry experiments. **c** FACS results for 3 whole genome CRISPRa screens with NTC sgRNA-transduced cells as negative controls. For screen 1, cells were incubated with Alexa Fluor 488-conjugated SARS-CoV-2 HexaPro Spike (Addgene #154754) and selected on puromycin for 3 days. For screen 2, cells were incubated with Alexa Fluor 488-conjugated SARS-CoV-2 Spike glycoprotein (residues 1-1208, complete ectodomain; gift from Dr. Florian Krammer) and selected on puromycin for 3 days. For screen 3, cells were incubated with Alexa Fluor 488-conjugated SARS-CoV-2 HexaPro spike (Addgene #15474) and selected on puromycin for 8 days.

Supplementary Fig. 2. CRISPR screen analysis and validation.

a-b Gene enrichment analysis of screens 2 (A) and 3 (B) performed using MAGeCK. Horizontal dotted line indicates p-value = 0.05. Vertical dotted line indicates log_2 fold changes (LFCs) of 2. P-values and LFCs for all genes in screens 2 and 3 are reported in **Supplementary Table 1. c-d** Density plot of Z-score (grey) for all sgRNA in (C) screen 2 and (D) screen 3. Blue vertical lines indicate Z-score for *ACE2* sgRNAs. Red vertical lines indicate Z-score for *LRRC15* sgRNAs. Z-scores calculated as described in methods. **e** Log_2 fold changes of all genes in Screen 1 vs. log_2 fold changes of all genes in Screen 2. **f** Log_2 fold changes of all genes in Screen 1 vs. log_2 fold changes of all genes in Screen 3. **g** *LRRC15* expression of cells in Fig 2e quantified via RT-qPCR. **h** *ACE2* expression was not increased in *LRRC15* sgRNA transduced cells (quantified via RT-qPCR). **i** The 3 sgRNAs for *ACE2* from the Calabrese library used in our screens were transduced into HEK293T-CRISPRa cells and *ACE2* expression was confirmed via qPCR. Only sgRNA3 induced upregulation in *ACE2* expression. **j** Transduced cells in **i** were incubated with Spike647 and analysed via flow cytometry. Only *ACE2* sgRNA3 cells showed a significant increase in Spike647 binding.

Supplementary Fig 3. LRRC15 is related to TLRs and interacts with Spike.

a Full phylogenetic tree of LRR-Tollkin family of proteins (includes fly and worm orthologs). **b** Co-immunoprecipitation of Spike was observed in LRRC15-GFP (transcripts 1 and 2) and ACE2 expressing cells but not in control GFP cells. I = input, FT = flow-through, E = elute. **c** Control rabbit IgG did not immunoprecipitate LRRC15 or Spike.

Supplementary Fig 4. LRRC15 expression inhibits SARS-CoV-2 Spike pseudovirus infection in ACE2 expressing cells. a SARS-CoV-2 pseudovirus carrying a firefly luciferase cassette was

applied to HEK293T, HEK293T-*ACE2* and HEK293T-*ACE2-TMPRSS2* cells for 24 hours before luminescence quantification. HEK293T cells were relatively resistant to infection while HEK293T-*ACE2* and HEK293T-*ACE2-TMPRSS2* expressing cells were infectable. N=3 for each condition. **b** Pseudovirus added to ACE2-expressing cells in the context of LRRC15. Titration of $15x10^6$, $62.5x10^6$, $250x10^6$ and $1000x10^6$ lentiviral particles in HEK293T-*ACE2* cells transfected with 0, 156.25, 312.5, 625, 1250 and 2500 ng of *Myc-DDK-tagged LRRC15* plasmid DNA. N=2 for each condition. **c-d** Luciferase assay for quantification of SARS-CoV-2 pseudovirus infection in **c** HEK293T-*ACE2* and **d** HEK293T-*ACE2-TMPRSS2* (N = 3). Cells were transfected with plasmid encoding *Myc-DDK-tagged LRRC15* transcript 1 or empty vector as a control. Luminescence for *LRRC15* cells were normalized to control cells. Significance was determined by two-way ANOVA, Sidak multiple comparison test; ****p<0.0001, ***p<0.001, **p<0.01, *p<0.05.

e Quantification of cell survival after incubation with authentic SARS-CoV-2 virus in HEK293T-*ACE2-TMPRSS2* cells transfected with plasmid encoding *Myc-DDK*-tagged *LRRC15* transcript 1 or *Myc-DDK* only (N = 3). Significance was determined by two-way ANOVA, *p<0.05.

Supplementary Fig 5. Single cell/nucleus analysis of different studies corroborates restricted *LRRC15* expression in fibroblasts.

a UMAP plot of lung single nucleus RNAseq dataset (Delorey et al). **b** Feature plot and **c** Dotplot shows *LRRC15* is expressed in Delorey et al. fibroblasts. **d** UMAP plot of lung single nucleus RNAseq dataset (Bharat et al). **e** Feature plot and **f** Dotplot shows *LRRC15* is expressed in Bharat et al. Lymphatic Endothelial cells and various populations of fibroblasts.

Supplementary Fig. 6. H&E and immunofluorescence staining of human lung tissue samples

Representative micrographs of **a** haematoxylin and eosin staining and **b** immunofluorescence staining of post-mortem formalin-fixed paraffin embedded human lung samples obtained from donors who died of severe COVID-19. Control samples were obtained from patients with melanoma metastases in the lung and non-tumor tissue used for comparisons. Micrographs taken at 200x magnification. Scale bar = 50 μM for **a**, 100 μM for **b**. In **b**, Red = Collagen I, Green = LRRC15, Blue = DAPI.

Supplementary Fig. 7. IMR90 fibroblasts bind SARS-CoV-2 Spike and *LRRC15* over-expressing fibroblasts show decreased Collagen VI expression

a Representative flow cytometry analysis of IMR90 fibroblasts incubated with Spike647 show cells have intrinsic Spike binding activity (N = 2). **b** Full images for LRRC15 and Collagen VI western blots. *LRRC15* overexpression in fibroblasts results in decreased Collagen VI protein expression.

Supplementary Table 1: CRISPR activation screen MAGeCK outputs.

Collated output of MAGeCK and MAGeCKFlute pipeline. For each screen, normalized read counts and Z-scores, gene-level summary, sgRNA-level summary and output of MAGeCKFlute ReadRRA() function is provided.

Supplementary Table 2: Oligonucleotides for CRISPR activation sgRNA constructs

Lists oligonucleotides used for generation of CRISPRa sgRNA constructs. Sequences for each sgRNA construct were from either Weismann lab Human Genome-wide CRISPRa-v2 Library (Addgene, #83978) or Calabrese Library Set A (Addgene, #92379).

Supplementary Table 3: Next Generation Sequencing Primers

List of primers used for next generation sequencing of gDNA extracted from pooled CRISPR activation screen samples. Primers were adapted from Sanson et al. [5].

Supplementary Table 4: RT-qPCR primer sequences

List of primers used for RT-qPCR.

Supplementary Table 5: Differential Gene Expression Analysis Results

Output of DRAGEN Differential Expression application.

Supplementary Table 6: **Ingenuity Comparison Analysis Canonical Pathways Results.**

Canonical pathways output from Ingenuity Comparison Analysis using DRAGEN Differential Expression results for IMR90 *TurboGFP* vs. IMR90 *LRRC15 T1-TurboGFP* for input.

References

1. Li, W. *et al.* Angiotensin-converting enzyme 2 is a functional receptor for the SARS coronavirus. *Nature* **426**, 450–454 (2003).
2. Kuba, K. *et al.* A crucial role of angiotensin converting enzyme 2 (ACE2) in SARS coronavirus-induced lung injury. *Nat. Med.* **11**, 875–879 (2005).
3. Zhou, P. *et al.* A pneumonia outbreak associated with a new coronavirus of probable bat origin. *Nature* **579**, 270–273 (2020).
4. Lu, R. *et al.* Genomic characterisation and epidemiology of 2019 novel coronavirus: implications for virus origins and receptor binding. *Lancet* **395**, 565–574 (2020).
5. Sanson, K. R. *et al.* Optimized libraries for CRISPR-Cas9 genetic screens with multiple modalities. *Nat. Commun.* **9**, 5416 (2018).
6. Horlbeck, M. A. *et al.* Compact and highly active next-generation libraries for CRISPR-mediated gene repression and activation. *Elife* **5**, (2016).
7. Li, W. *et al.* MAGeCK enables robust identification of essential genes from genome-scale CRISPR/Cas9 knockout screens. *Genome Biol.* **15**, 554 (2014).
8. Wang, B. *et al.* Integrative analysis of pooled CRISPR genetic screens using MAGeCKFlute. *Nat. Protoc.* **14**, 756–780 (2019).
9. Lan, J. *et al.* Structure of the SARS-CoV-2 spike receptor-binding domain bound to the ACE2 receptor. *Nature* **581**, 215–220 (2020).
10. Wrapp, D. *et al.* Cryo-EM structure of the 2019-nCoV spike in the prefusion conformation. *Science* **367**, 1260–1263 (2020).
11. Wang, Q. *et al.* Structural and Functional Basis of SARS-CoV-2 Entry by Using Human ACE2. *Cell* **181**, 894–904.e9 (2020).

12. Dolan, J. *et al.* The extracellular leucine-rich repeat superfamily; a comparative survey and analysis of evolutionary relationships and expression patterns. *BMC Genomics* **8**, 320 (2007).
13. Hsieh, C.-L. *et al.* Structure-based design of prefusion-stabilized SARS-CoV-2 spikes. *Science* **369**, 1501–1505 (2020).
14. Uhlén, M. *et al.* Proteomics. Tissue-based map of the human proteome. *Science* **347**, 1260419 (2015).
15. Vento-Tormo, R. *et al.* Single-cell reconstruction of the early maternal-fetal interface in humans. *Nature* **563**, 347–353 (2018).
16. Huang, N. *et al.* SARS-CoV-2 infection of the oral cavity and saliva. *Nat. Med.* **27**, 892–903 (2021).
17. Madissoon, E. *et al.* scRNA-seq assessment of the human lung, spleen, and esophagus tissue stability after cold preservation. *Genome Biol.* **21**, 1 (2019).
18. Park, J.-E. *et al.* A cell atlas of human thymic development defines T cell repertoire formation. *Science* **367**, (2020).
19. Martin, J. C. *et al.* Single-Cell Analysis of Crohn's Disease Lesions Identifies a Pathogenic Cellular Module Associated with Resistance to Anti-TNF Therapy. *Cell* **178**, 1493–1508.e20 (2019).
20. Solé-Boldo, L. *et al.* Single-cell transcriptomes of the human skin reveal age-related loss of fibroblast priming. *Commun Biol* **3**, 188 (2020).
21. Henry, G. H. *et al.* A Cellular Anatomy of the Normal Adult Human Prostate and Prostatic Urethra. *Cell Rep.* **25**, 3530–3542.e5 (2018).
22. Vieira Braga, F. A. *et al.* A cellular census of human lungs identifies novel cell states in health and in asthma. *Nat. Med.* **25**, 1153–1163 (2019).
23. Buechler, M. B. *et al.* Cross-tissue organization of the fibroblast lineage. *Nature* **593**, 575–579 (2021).
24. Delorey, T. M. *et al.* COVID-19 tissue atlases reveal SARS-CoV-2 pathology and cellular targets. *Nature* **595**, 107–113 (2021).
25. Bharat, A. *et al.* Lung transplantation for patients with severe COVID-19. *Sci. Transl. Med.* **12**,

(2020).

26. Melms, J. C. *et al.* A molecular single-cell lung atlas of lethal COVID-19. *Nature* **595**, 114–119 (2021).

27. Satoh, K., Hata, M. & Yokota, H. A novel member of the leucine-rich repeat superfamily induced in rat astrocytes by beta-amyloid. *Biochem. Biophys. Res. Commun.* **290**, 756–762 (2002).

28. Dominguez, C. X. *et al.* Single-Cell RNA Sequencing Reveals Stromal Evolution into LRRC15+ Myofibroblasts as a Determinant of Patient Response to Cancer Immunotherapy. *Cancer Discov.* **10**, 232–253 (2020).

29. Krishnamurty, A. T. *et al.* LRRC15+ myofibroblasts dictate the stromal setpoint to suppress tumour immunity. *Nature* (2022) doi:10.1038/s41586-022-05272-1.

30. O'Prey, J., Wilkinson, S. & Ryan, K. M. Tumor antigen LRRC15 impedes adenoviral infection: implications for virus-based cancer therapy. *J. Virol.* **82**, 5933–5939 (2008).

31. Hayashi, F. *et al.* The innate immune response to bacterial flagellin is mediated by Toll-like receptor 5. *Nature* **410**, 1099–1103 (2001).

32. Shilts, J. *et al.* LRRC15 mediates an accessory interaction with the SARS-CoV-2 spike protein. bioRxiv 2021.09.25.461776; doi: https://doi.org/10.1101/2021.09.25.461776. *bioRxiv* 2021.09.25.461776 (2021) doi:10.1101/2021.09.25.461776.

33. Song, J. *et al.* LRRC15 inhibits SARS-CoV-2 cellular entry in trans. *PLoS Biol.* **20**, e3001805 (2022).

34. Loo, L. *et al.* LRRC15 suppresses SARS-CoV-2 infection and controls collagen production. *bioRxiv* 2021.11.09.467981 (2021) doi:10.1101/2021.11.09.467981.

35. Zhu, S. *et al.* Genome-wide CRISPR activation screen identifies candidate receptors for SARS-CoV-2 entry. *Sci. China Life Sci.* (2021) doi:10.1007/s11427-021-1990-5.

36. Schneider, W. M. *et al.* Genome-Scale Identification of SARS-CoV-2 and Pan-coronavirus Host Factor Networks. *Cell* **184**, 120–132.e14 (2021).

37. Baggen, J. *et al.* Genome-wide CRISPR screening identifies TMEM106B as a proviral host factor

for SARS-CoV-2. *Nat. Genet.* **53**, 435–444 (2021).

38. Wang, R. *et al.* Genetic Screens Identify Host Factors for SARS-CoV-2 and Common Cold Coronaviruses. *Cell* **184**, 106–119.e14 (2021).

39. Goujon, C. *et al.* Bidirectional genome-wide CRISPR screens reveal host factors regulating SARS-CoV-2, MERS-CoV and seasonal HCoVs. *Res Sq* (2021) doi:10.21203/rs.3.rs-555275/v1.

40. Wei, J. *et al.* Genome-wide CRISPR Screens Reveal Host Factors Critical for SARS-CoV-2 Infection. *Cell* **184**, 76–91.e13 (2021).

41. Daniloski, Z. *et al.* Identification of Required Host Factors for SARS-CoV-2 Infection in Human Cells. *Cell* **184**, 92–105.e16 (2021).

42. Singh, D. K. *et al.* Myeloid cell interferon responses correlate with clearance of SARS-CoV-2. *Nat. Commun.* **13**, 679 (2022).

43. Yoshida, M. *et al.* Local and systemic responses to SARS-CoV-2 infection in children and adults. *Nature* **602**, 321–327 (2022).

44. Abbas, Y. M., Pichlmair, A., Górna, M. W., Superti-Furga, G. & Nagar, B. Structural basis for viral 5'-PPP-RNA recognition by human IFIT proteins. *Nature* **494**, 60–64 (2013).

45. Schindewolf, C. *et al.* SARS-CoV-2 uses nonstructural protein 16 to evade restriction by IFIT1 and IFIT3. *bioRxivorg* (2022) doi:10.1101/2022.09.26.509529.

46. Gao, S. *et al.* Structural basis of oligomerization in the stalk region of dynamin-like MxA. *Nature* **465**, 502–506 (2010).

47. Bizzotto, J. *et al.* SARS-CoV-2 Infection Boosts MX1 Antiviral Effector in COVID-19 Patients. *iScience* **23**, 101585 (2020).

48. Schroeder, S. *et al.* Interferon antagonism by SARS-CoV-2: a functional study using reverse genetics. *Lancet Microbe* **2**, e210–e218 (2021).

49. Donovan, J., Dufner, M. & Korennykh, A. Structural basis for cytosolic double-stranded RNA surveillance by human oligoadenylate synthetase 1. *Proc. Natl. Acad. Sci. U. S. A.* **110**, 1652–1657 (2013).

50. Wickenhagen, A. *et al.* A prenylated dsRNA sensor protects against severe COVID-19. *Science* **374**, eabj3624 (2021).

51. Gisby, J. S. *et al.* Multi-omics identify LRRC15 as a COVID-19 severity predictor and persistent pro-thrombotic signals in convalescence. *bioRxiv* (2022) doi:10.1101/2022.04.29.22274267.

52. Rendeiro, A. F. *et al.* The spatial landscape of lung pathology during COVID-19 progression. *Nature* **593**, 564–569 (2021).

53. Tea, F. *et al.* SARS-CoV-2 neutralizing antibodies: Longevity, breadth, and evasion by emerging viral variants. *PLoS Med.* **18**, e1003656 (2021).

54. Follenzi, A. *et al.* Targeting lentiviral vector expression to hepatocytes limits transgene-specific immune response and establishes long-term expression of human antihemophilic factor IX in mice. *Blood* **103**, 3700–3709 (2004).

55. Aggarwal, A. *et al.* Mobilization of HIV spread by diaphanous 2 dependent filopodia in infected dendritic cells. *PLoS Pathog.* **8**, e1002762 (2012).

56. Jumper, J. *et al.* Highly accurate protein structure prediction with AlphaFold. *Nature* **596**, 583–589 (2021).

57. UniProt Consortium. UniProt: the universal protein knowledgebase in 2021. *Nucleic Acids Res.* **49**, D480–D489 (2021).

58. Sievers, F. *et al.* Fast, scalable generation of high-quality protein multiple sequence alignments using Clustal Omega. *Mol. Syst. Biol.* **7**, 539 (2011).

59. Stecher, G., Tamura, K. & Kumar, S. Molecular Evolutionary Genetics Analysis (MEGA) for macOS. *Mol. Biol. Evol.* **37**, 1237–1239 (2020).

60. Hao, Y. *et al.* Integrated analysis of multimodal single-cell data. *Cell* **184**, 3573–3587.e29 (2021).

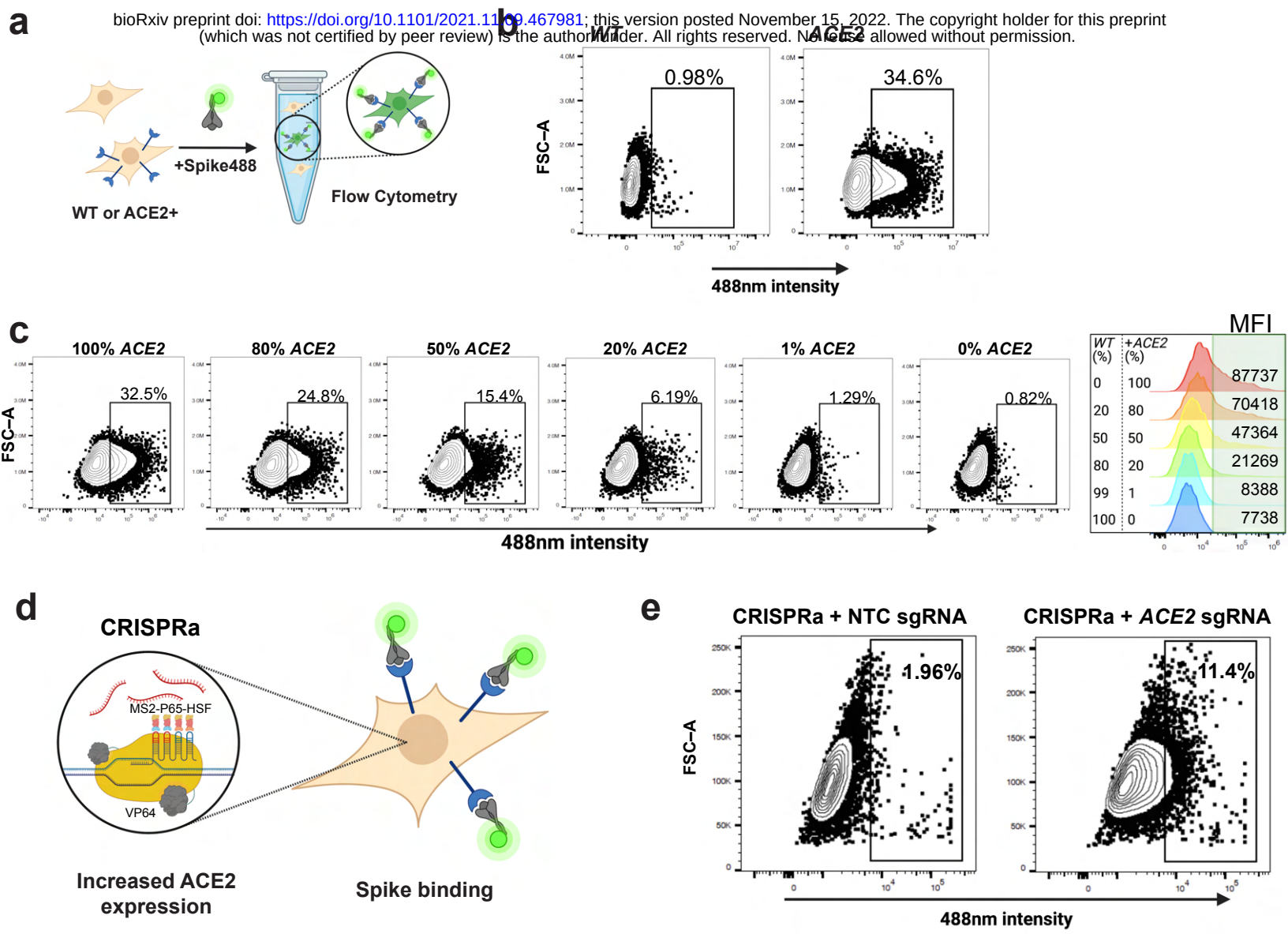

Figure 1

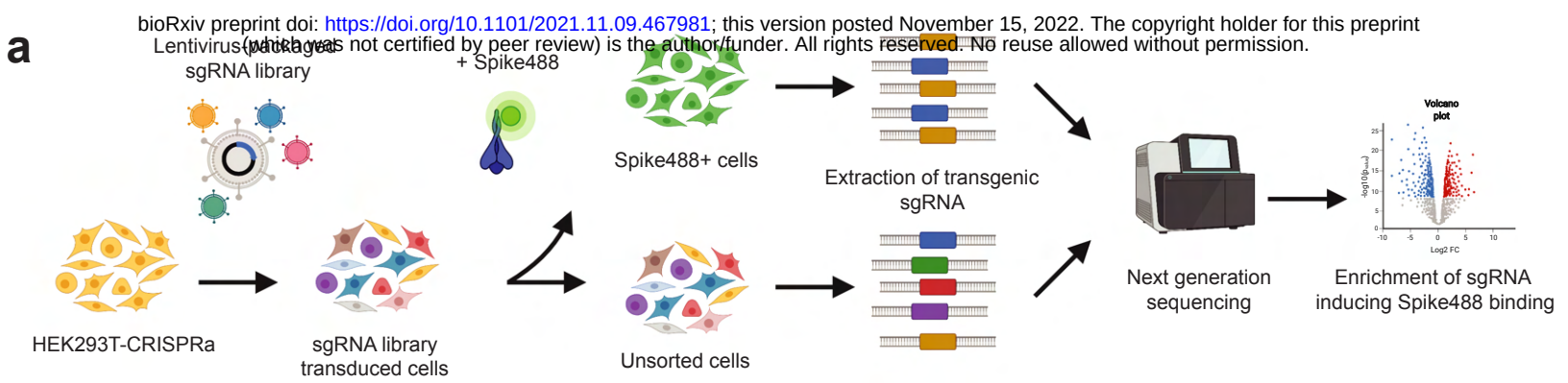

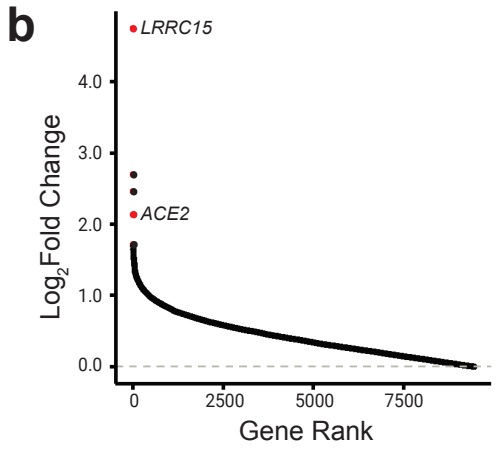

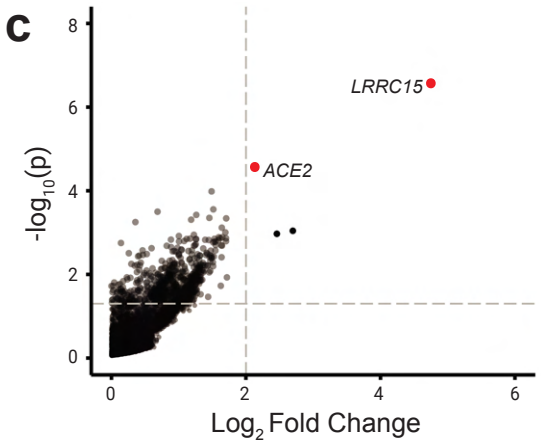

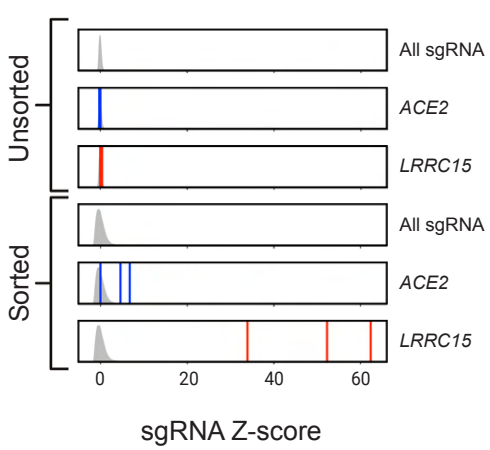

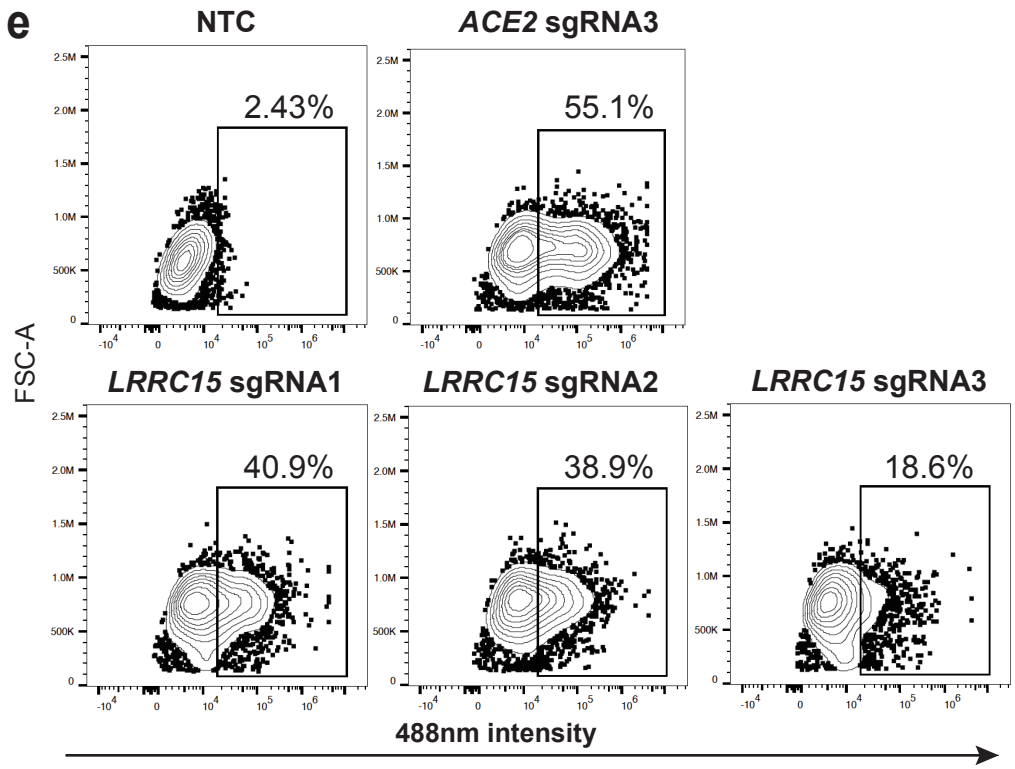

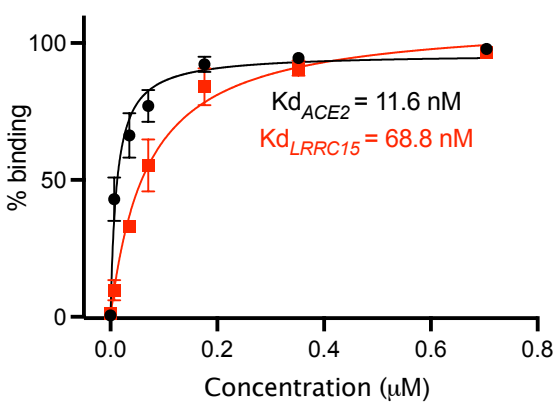

Figure 2

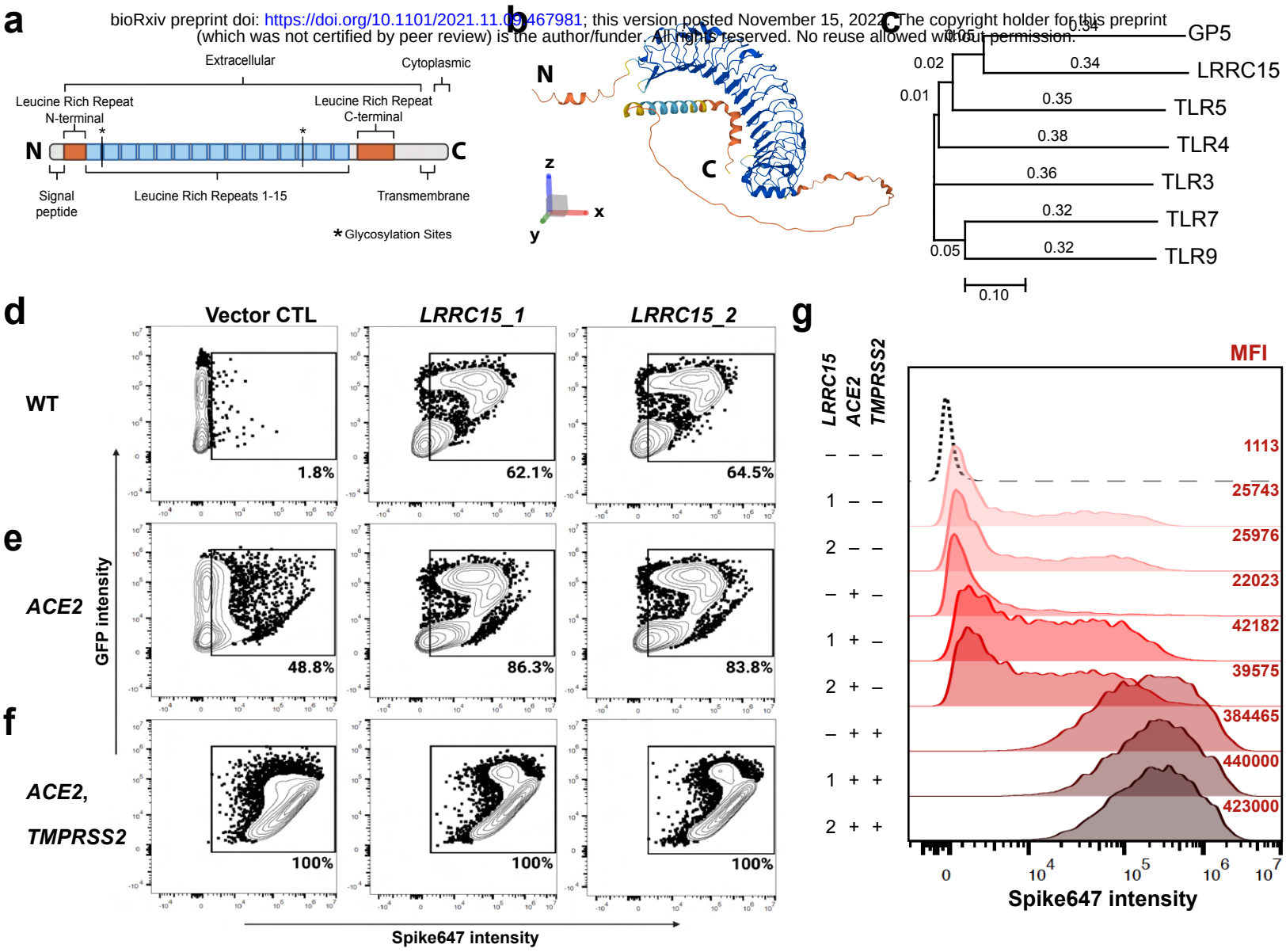

Figure 3

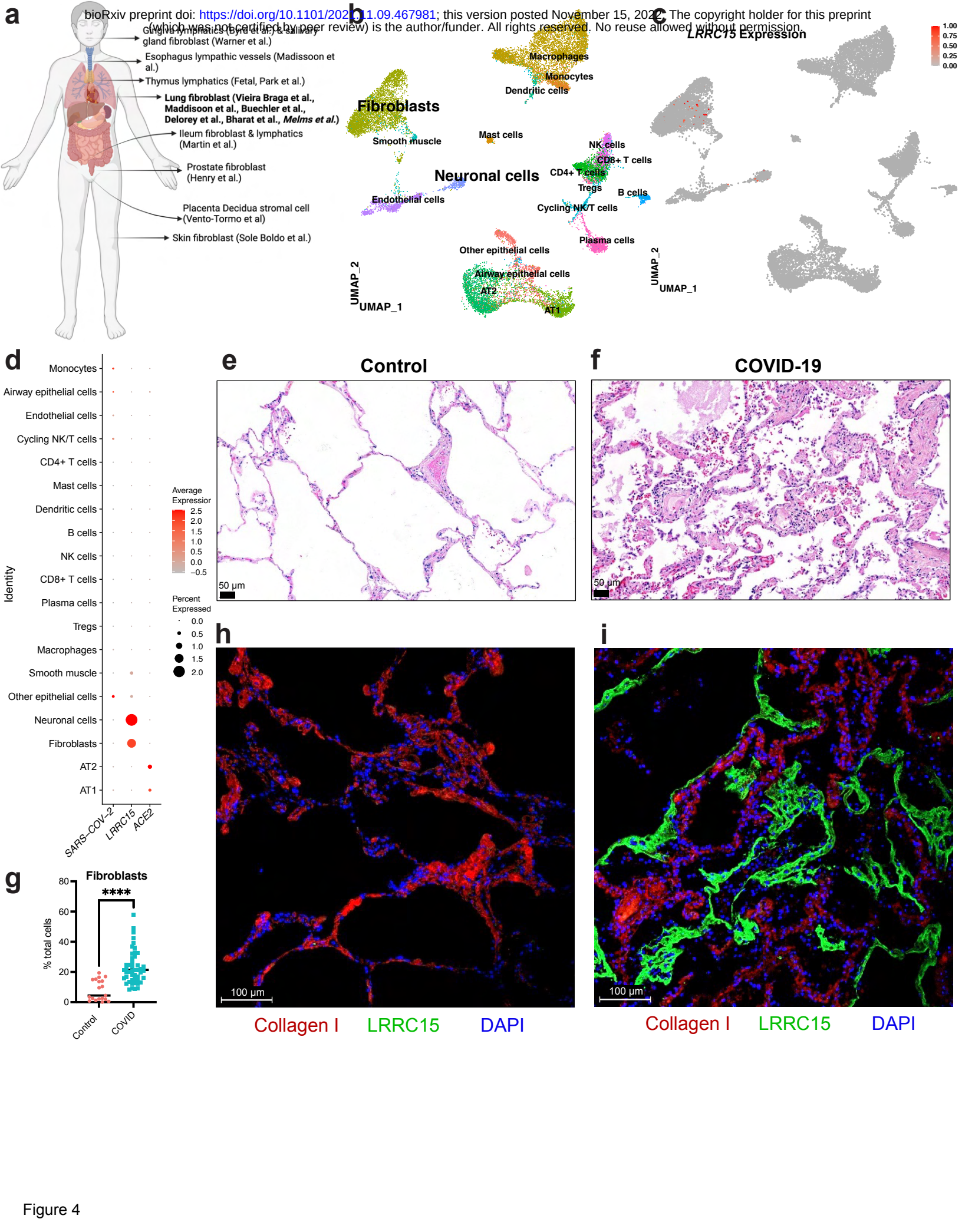

Figure 4

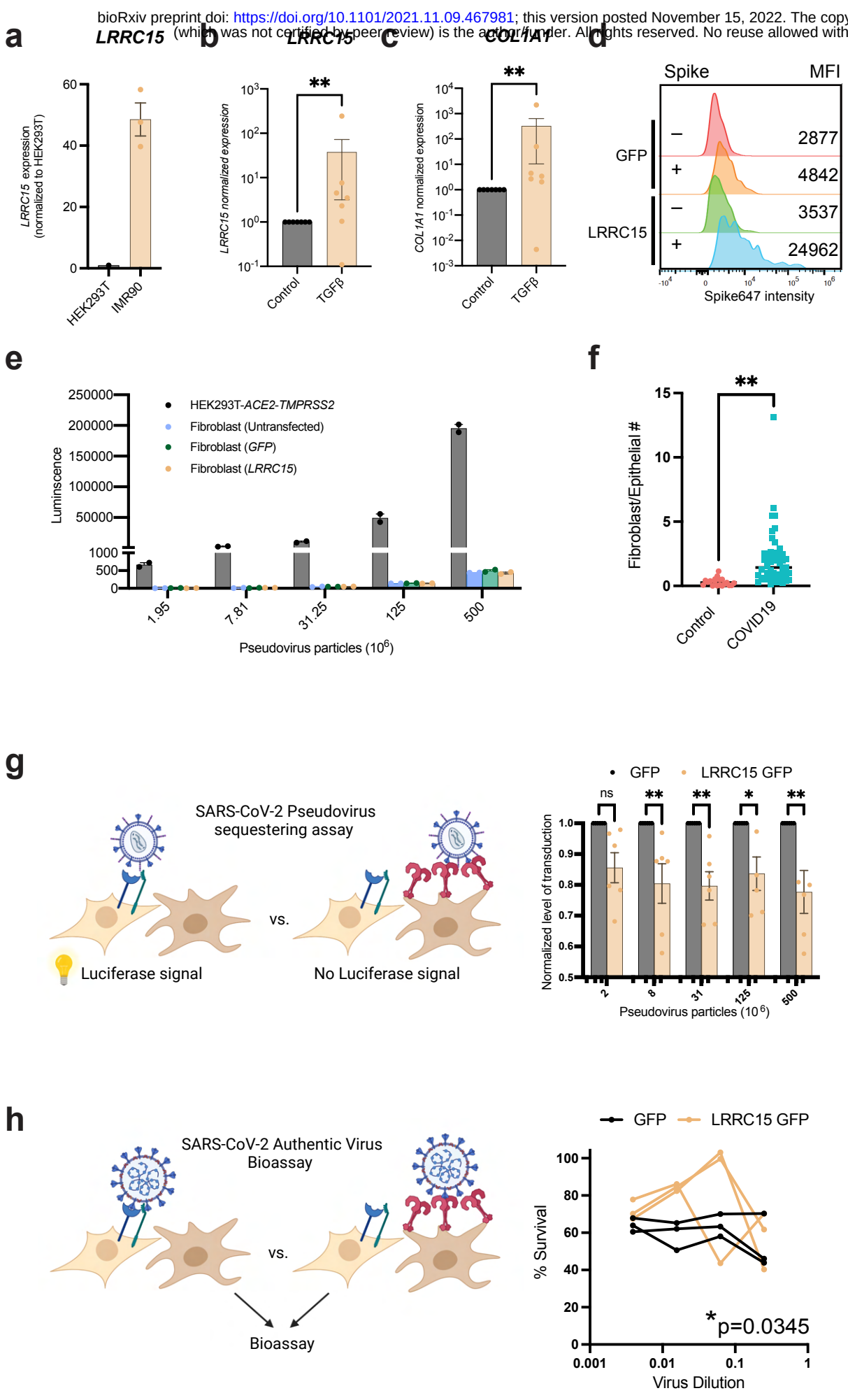

Figure 5

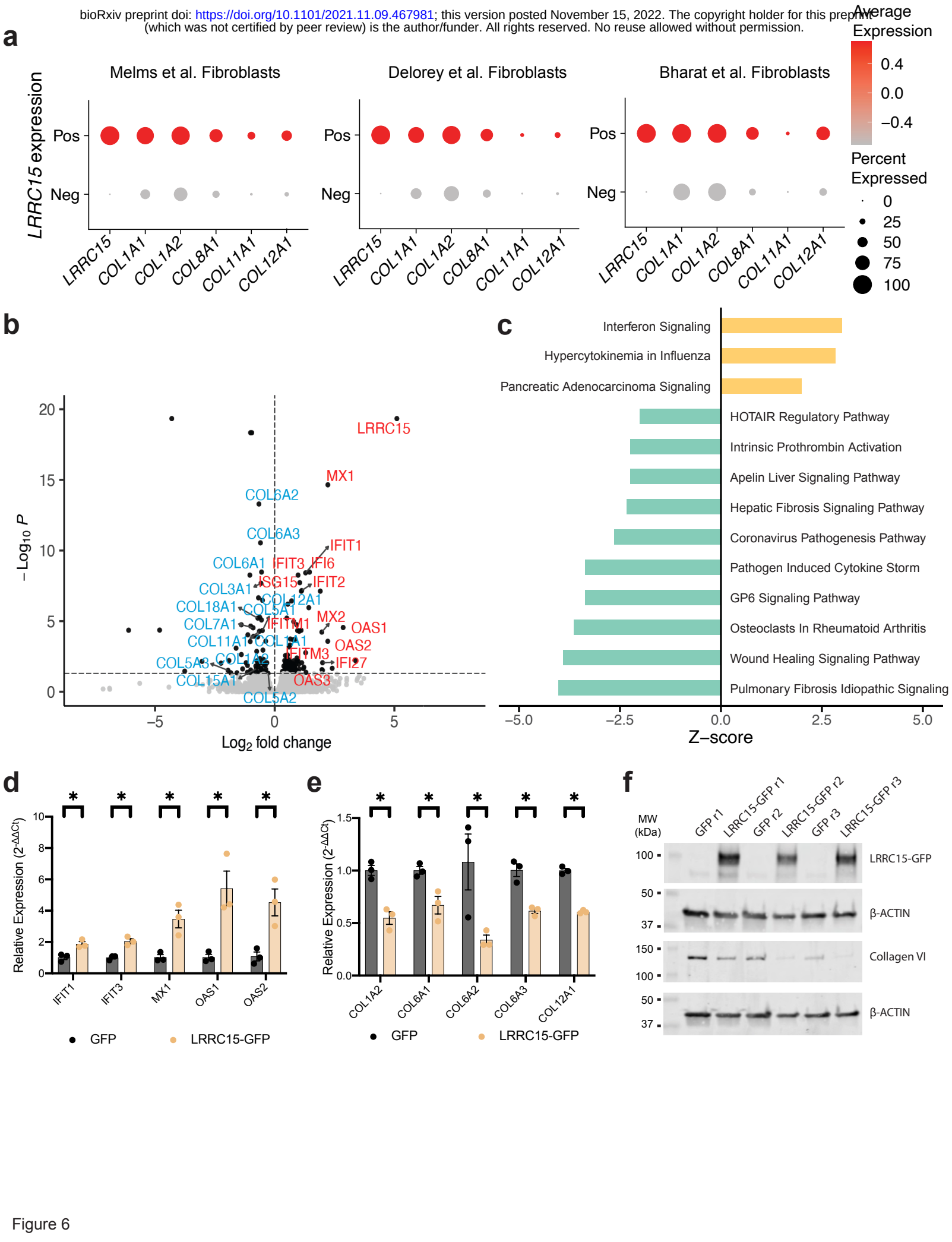

Figure 6

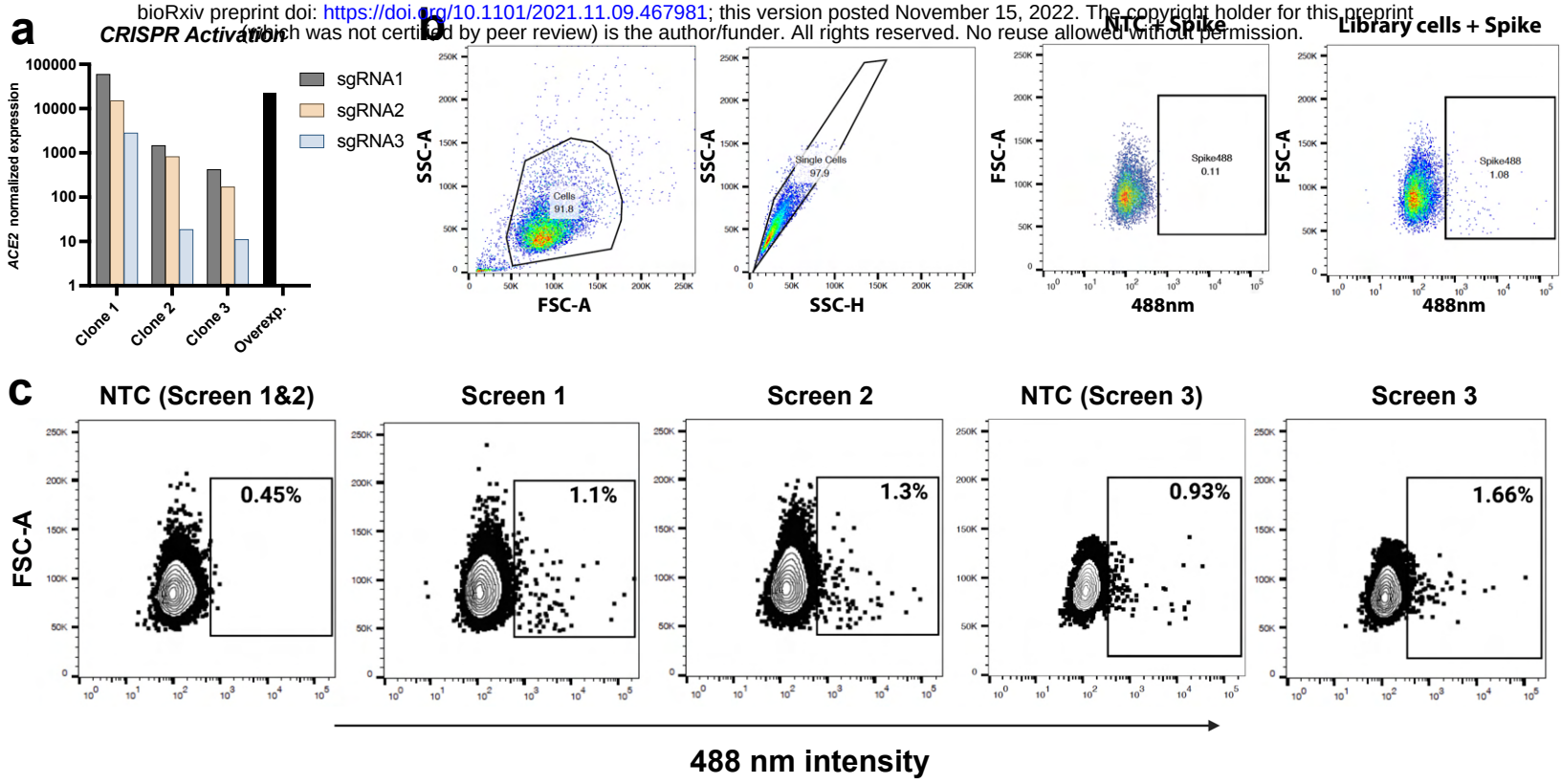

Supplementary Figure 1

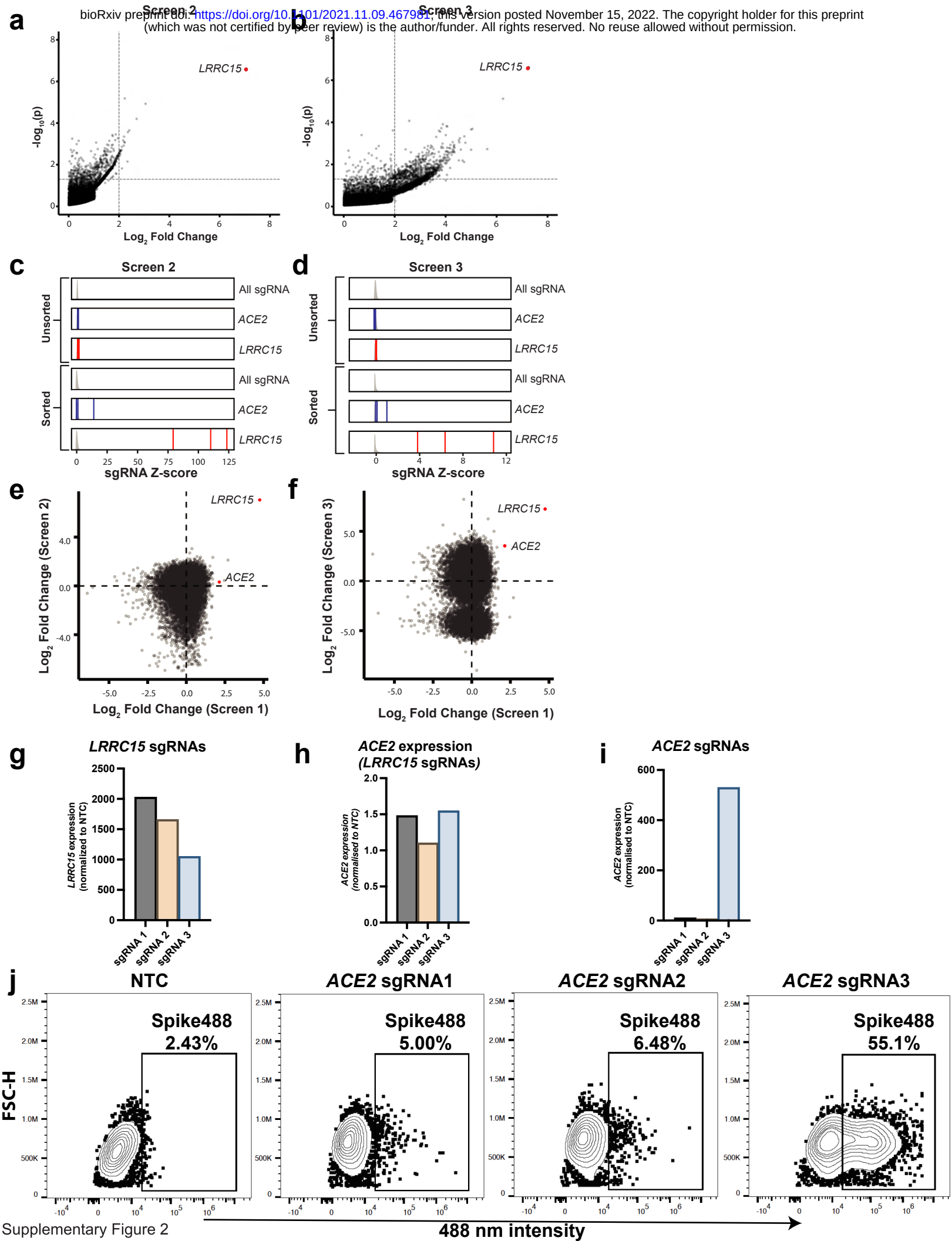

Supplementary Figure 2

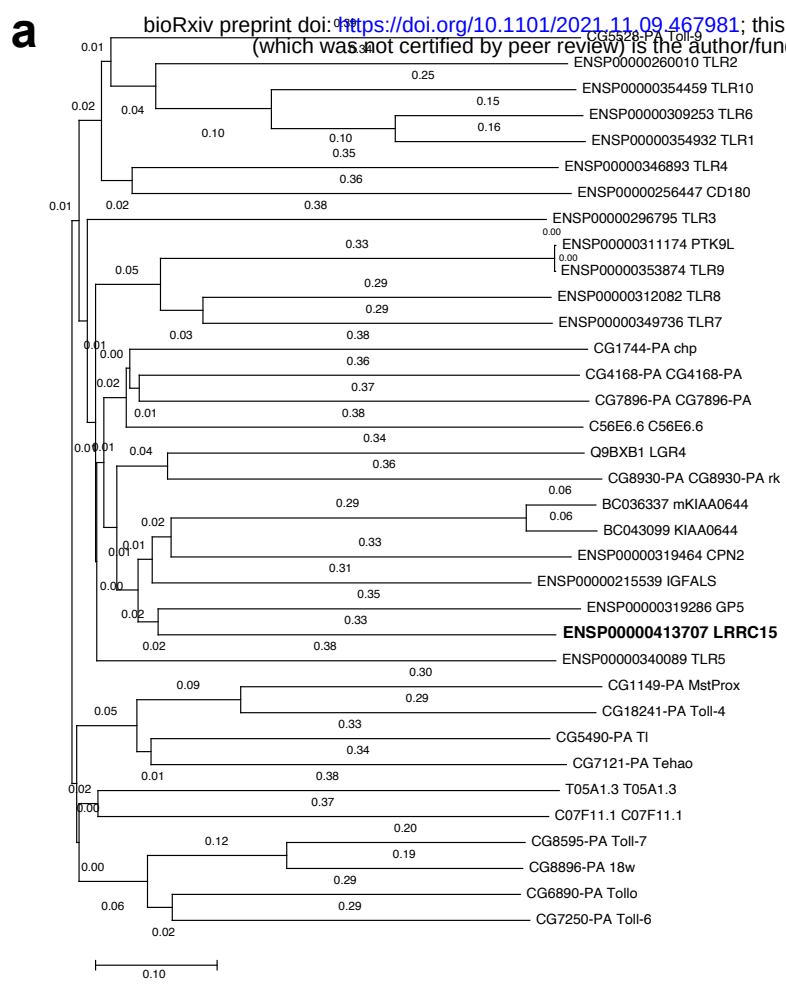

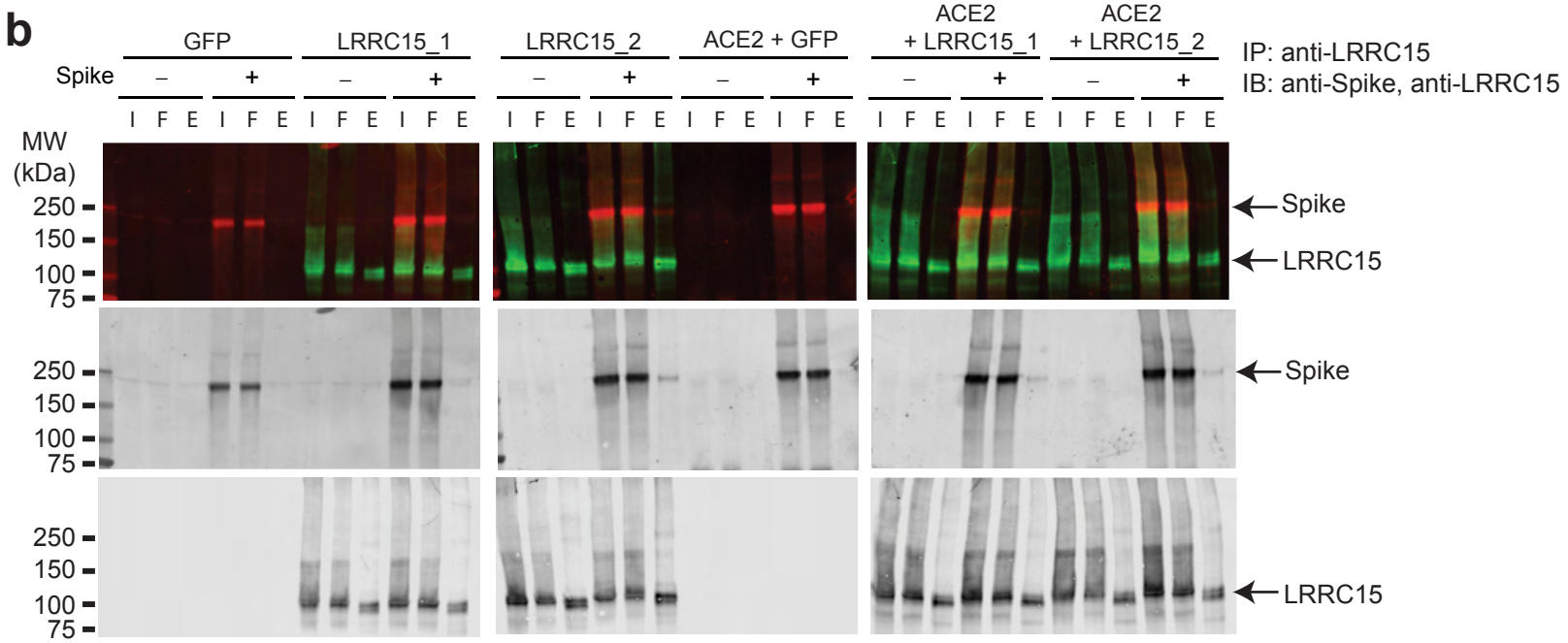

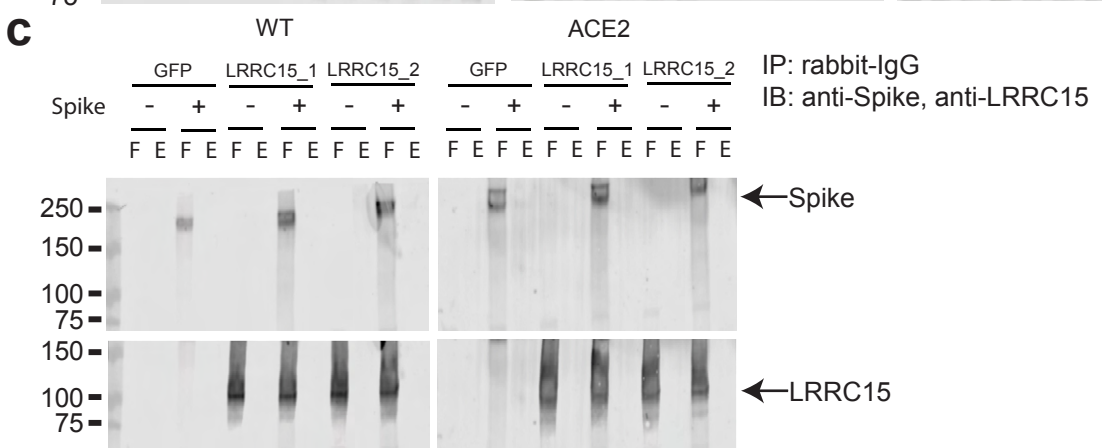

Supplementary Figure 3

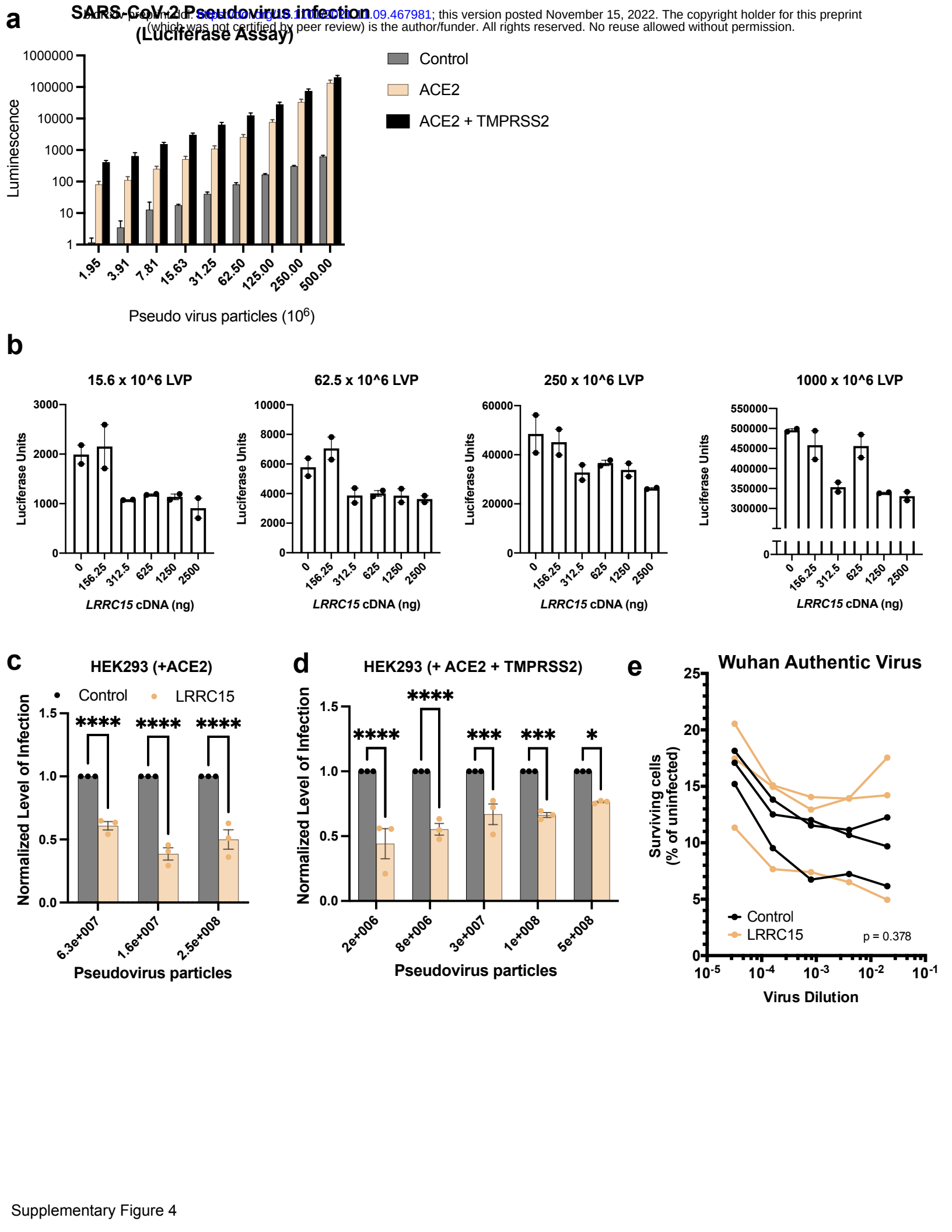

Supplementary Figure 4

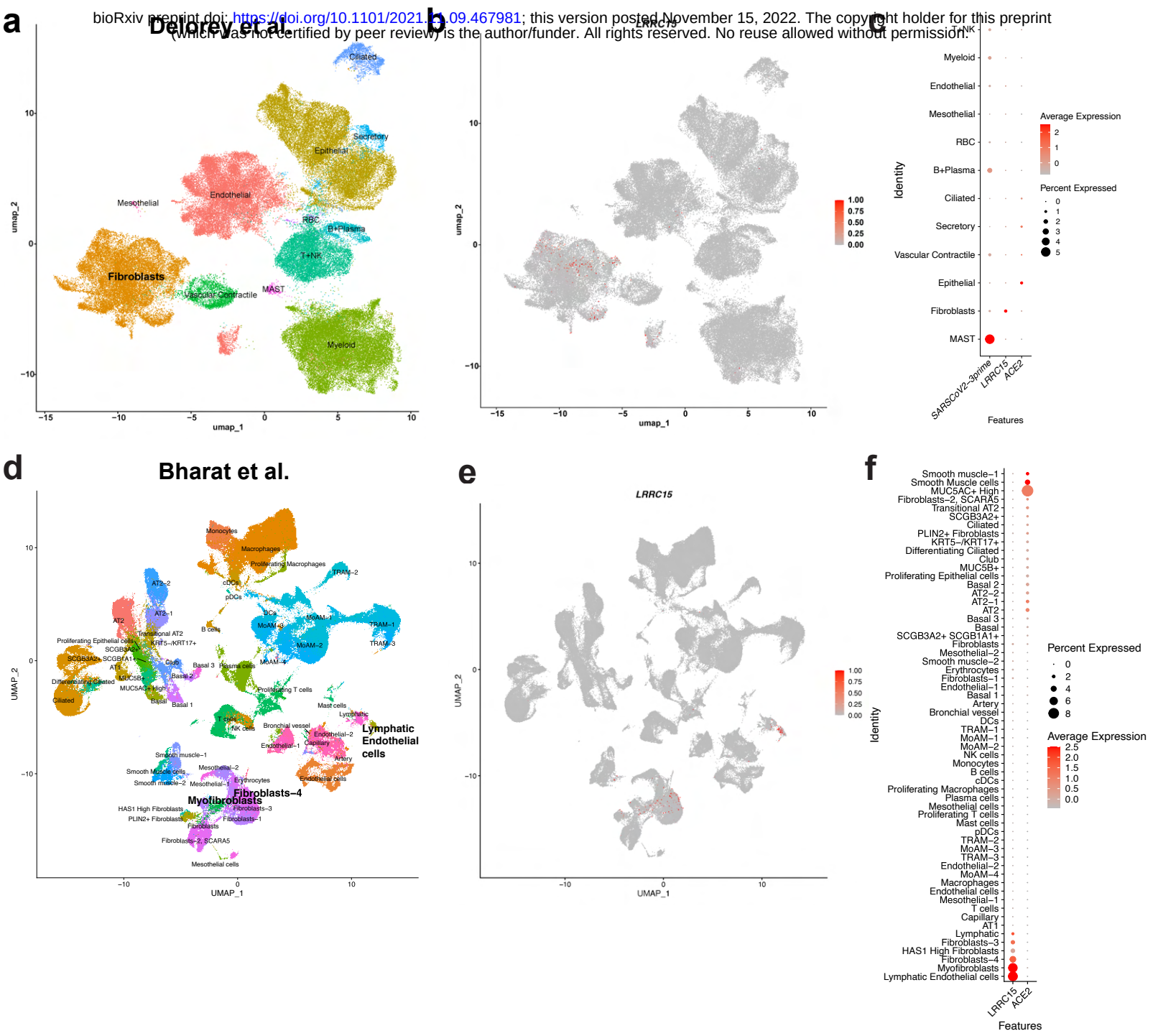

Supplementary Figure 5

a

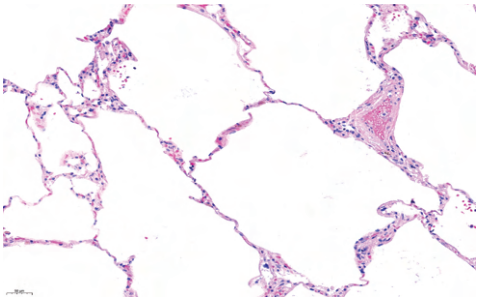

Control

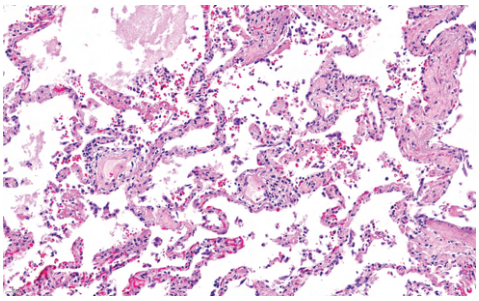

COVID 1

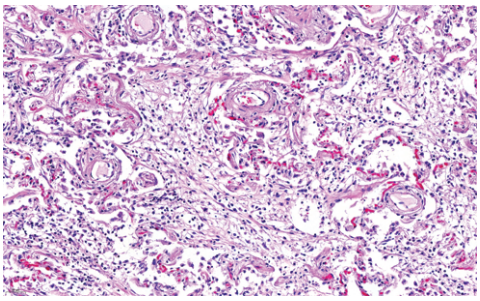

COVID 2

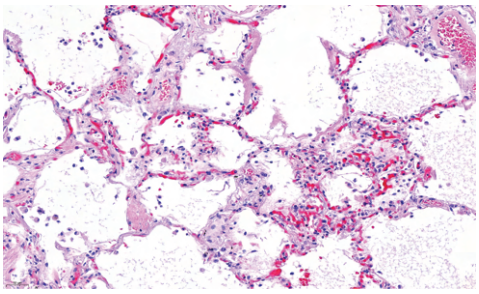

COVID 3

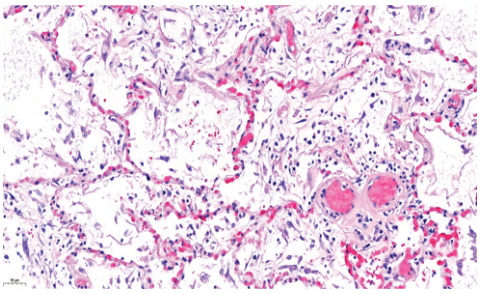

COVID 4

b

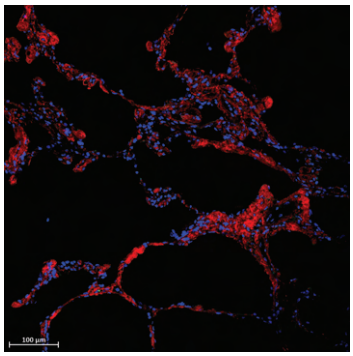

Control 1

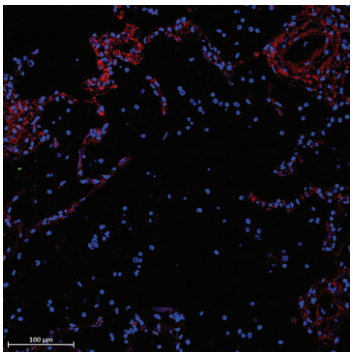

Control 2

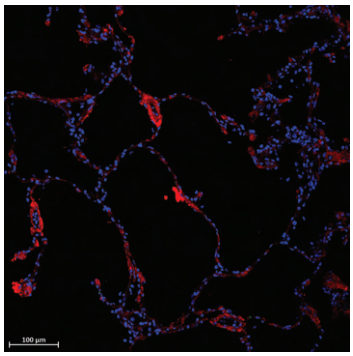

Control 3

Collagen I

LRRC15

DAPI

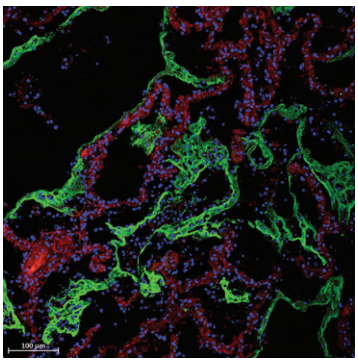

COVID 1

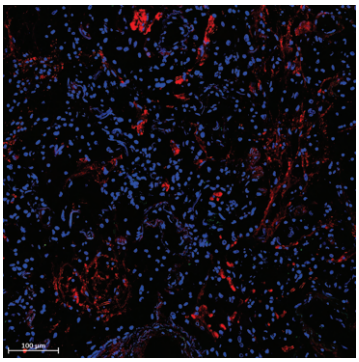

COVID 2

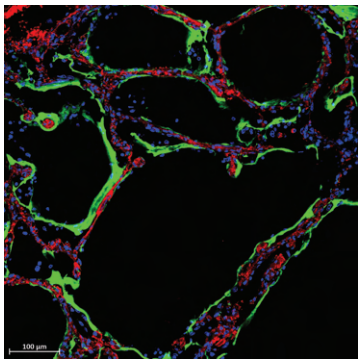

COVID 3

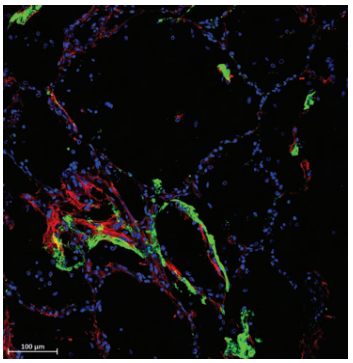

COVID 4

Supplementary Figure 6

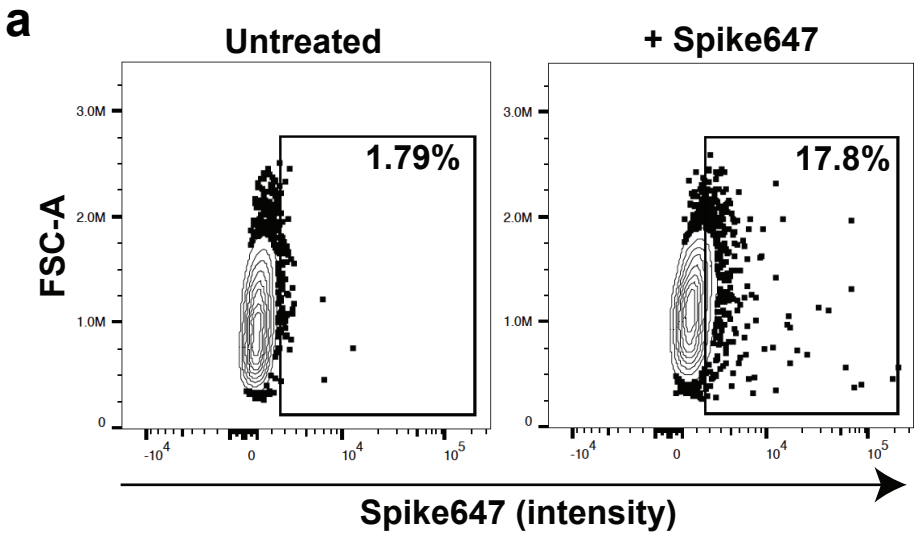

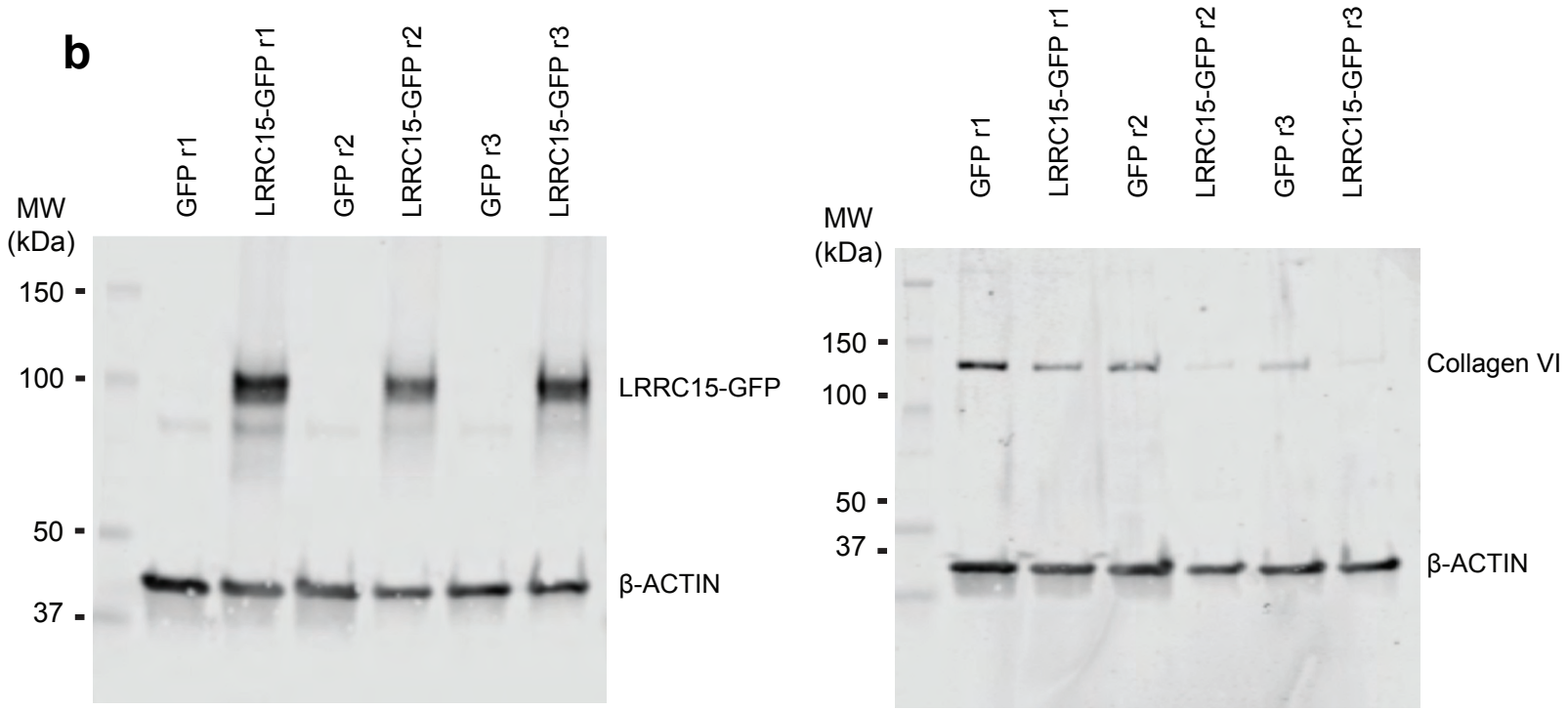

Supplementary Figure 7